(12) INTERNATIONAL APPLICATION PUBLISHED UNDER THE PATENT COOPERATION TREATY (PCT)

(19) World Intellectual Property Organization
International Bureau

(43) International Publication Date
13 September 2018 (13.09.2018)

WIPO | PCT

(10) International Publication Number
WO 2018/165117 A1

(51) International Patent Classification:
*G02B 27/01* (2006.01) *G02B 27/10* (2006.01)
*G02B 17/08* (2006.01) *G02B 27/22* (2018.01)

(21) International Application Number:
PCT/US2018/021087

(22) International Filing Date:
06 March 2018 (06.03.2018)

(25) Filing Language: English

(26) Publication Language: English

(30) Priority Data:
62/469,097 09 March 2017 (09.03.2017) US

(71) Applicant: **ARIZONA BOARD OF REGENTS ON BEHALF OF THE UNIVERSITY OF ARIZONA** [US/US]; Tech Transfer Arizona, 220 West Sixth Street, 4th Floor, Tucson, AZ 85701 (US).

(72) Inventors: **HUA, Hong**; 1630 E University Blvd, Tucson, AZ 85721 (US). **HUANG, Hekun**; 6580 N. Calle Sin Nombre, Tucson, AZ 85718 (US).

(74) Agent: **HAUN, Niels** et al.; Dann, Dorfman, Herrell and Skilliman, P.C., 1601 Market Street, Suite 2400, Philadelphia, PA 19103 (US).

(81) Designated States *(unless otherwise indicated, for every kind of national protection available)*: AE, AG, AL, AM, AO, AT, AU, AZ, BA, BB, BG, BH, BN, BR, BW, BY, BZ, CA, CH, CL, CN, CO, CR, CU, CZ, DE, DJ, DK, DM, DO, DZ, EC, EE, EG, ES, FI, GB, GD, GE, GH, GM, GT, HN, HR, HU, ID, IL, IN, IR, IS, JO, JP, KE, KG, KH, KN, KP, KR, KW, KZ, LA, LC, LK, LR, LS, LU, LY, MA, MD, ME, MG, MK, MN, MW, MX, MY, MZ, NA, NG, NI, NO, NZ, OM, PA, PE, PG, PH, PL, PT, QA, RO, RS, RU, RW, SA, SC, SD, SE, SG, SK, SL, SM, ST, SV, SY, TH, TJ, TM, TN, TR, TT, TZ, UA, UG, US, UZ, VC, VN, ZA, ZM, ZW.

(84) Designated States *(unless otherwise indicated, for every kind of regional protection available)*: ARIPO (BW, GH, GM, KE, LR, LS, MW, MZ, NA, RW, SD, SL, ST, SZ, TZ, UG, ZM, ZW), Eurasian (AM, AZ, BY, KG, KZ, RU, TJ, TM), European (AL, AT, BE, BG, CH, CY, CZ, DE, DK, EE, ES, FI, FR, GB, GR, HR, HU, IE, IS, IT, LT, LU, LV, MC, MK, MT, NL, NO, PL, PT, RO, RS, SE, SI, SK, SM, TR), OAPI (BF, BJ, CF, CG, CI, CM, GA, GN, GQ, GW, KM, ML, MR, NE, SN, TD, TG).

**Published:**
— *with international search report (Art. 21(3))*

(54) Title: HEAD-MOUNTED LIGHT FIELD DISPLAY WITH INTEGRAL IMAGING AND RELAY OPTICS

FIG.3A

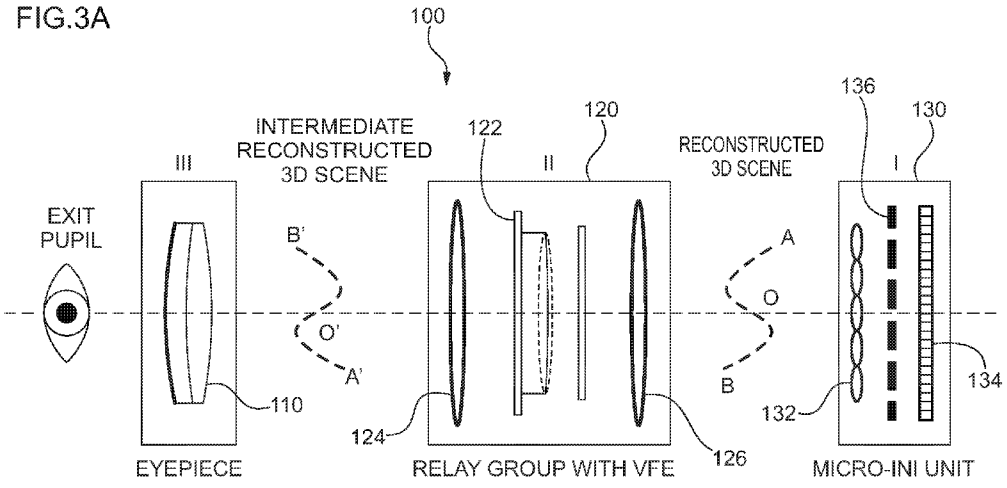


(57) Abstract: Head-mounted light field display with integral imaging and relay group.

WO 2018/165117 A1

# HEAD-MOUNTED LIGHT FIELD DISPLAY WITH INTEGRAL IMAGING AND RELAY OPTICS

## RELATED APPLICATIONS

This application claims the benefit of priority of U.S. Provisional Application No. 62/469,097, filed on March 9, 2017, the entire contents of which application are incorporated herein by reference.

## GOVERNMENT LICENSE RIGHTS

This invention was made with government support under Grant No. 1422653 awarded by the NSF. The government has certain rights in the invention.

## FIELD OF THE INVENTION

The present invention relates generally to the field of head-mounted displays, and more particularly, but not exclusively to head-mounted displays based on integral imaging (InI).

## BACKGROUND

Head-mounted displays (HMD), also commonly known as near-to-eye displays (NED) or head-worn displays (HWD), have gained significant interest in recent years and stimulated tremendous efforts to push the technology forward for a broad range of consumer applications. For instance, a lightweight optical see-through HMD (OST-HMD), which enables optical superposition of digital information onto a user's direct view of the physical world and maintains see-through vision to the real-world, is one of the key enabling technologies to augmented reality (AR) applications. A wide field-of-view (FOV), immersive HMD, which immerses a user in computer-generated virtual world or a high-resolution video capture of a remote real-world, is a key enabling technology to virtual reality (VR) applications. HMDs find a myriad of applications in gaming, simulation and training, defense, education, and other fields.

Despite the high promises and the tremendous progress made recently toward the development of both VR and AR displays, minimizing visual discomfort involved in wearing HMDs for an extended period remains an unresolved challenge. One of the key contributing factors to visual discomfort is the vergence-accommodation conflicts (VAC) due to the lack of the ability to render correct focus cues, including accommodation cue and retinal image blur effects. The VAC problem in HMDs stems from the fact that the image source is mostly a 2D flat surface located at a fixed distance from the eye. Figure 1 shows a schematic layout of a

typical monocular HMD, which mainly includes a 2D microdisplay as the image source and an eyepiece that magnifies the image rendered on the microdisplay and forms a virtual image appearing at a fixed distance from the eye. An OST-HMD requires an optical combiner (e.g. beamsplitter) placed in front of the eye to combine the optical paths of the virtual display and real scene. The conventional HMDs, whether monocular or binocular, see-through or immersive, lack the ability to render correct focus cues for the digital information which may appear at other distances than that corresponding to the virtual image plane. As a result, conventional HMDs fail to stimulate natural eye accommodation response and retinal blurry effects. The problem of lacking correct focus cues in HMDs causes several visual cue conflicts. For instance, a conventional stereoscopic HMD stimulates the perception of 3D space and shapes from a pair of two-dimensional (2D) perspective images, one for each eye, with binocular disparities and other pictorial depth cues of a 3D scene seen from two slightly different viewing positions. Therefore, conventional stereoscopic HMDs force an unnatural decoupling of the accommodation and convergence cues. The cue for the accommodation depth is dictated by the depth of the 2D image plane while the convergence depth of the 3D scene is dictated by the binocular disparities rendered by the image pair. The retinal image blurring cues for virtual objects rendered by the display is mismatched from those created by the natural scene. Many studies have provided strong supportive evidence that these conflicting visual cues related to incorrectly rendered focus cues in conventional HMDs may contribute to various visual artifacts and degraded visual performance.

Several approaches proposed previously may overcome the drawbacks of conventional stereoscopic displays, including volumetric displays, super-multi-view auto-stereoscopic displays, Integral-Imaging-based displays, holographic displays, multi-focal-plane displays, and computational multi-layer displays. Due to their enormous hardware complexity, many of these different display methods are not suitable for implementation in HMD systems. On the other hand, the multi-focal-plane display, integral-imaging, and computational multi-layer approaches are commonly referred to be light field displays and are suitable for head-mounted applications. Their use in HMDs is referred to as head-mounted light field displays.

Head-mounted light field displays render a true 3D scene by sampling either the projections of the 3D scene at different depths or the directions of the light rays apparently emitted by the 3D scene and viewed from different eye positions. They are capable of rendering correct or nearly

correct focus cues and addressing the vergence-accommodation mismatch problem in conventional VR and AR displays. For instance, an integral imaging (InI) based display reconstructs the light fields of a 3D scene by angularly sampling the directions of the light rays apparently emitted by the 3D scene and viewed from different eye positions. As illustrated in Fig. 2, a simple InI-based display typically includes a display panel and a 2D array which can be a microlens array (MLA) or pinhole array. The display renders a set of 2D elemental images, each of which represents a different perspective of a 3D scene. The conical ray bundles emitted by the corresponding pixels in the elemental images intersect and integrally create the perception of a 3D scene that appears to emit light and occupy the 3D space. The InI-based display using 2D arrays allows the reconstruction of a 3D shape with full-parallax information in both horizontal and vertical directions, which is its main difference from the conventional auto-stereoscopic displays with only horizontal parallax using one-dimensional parallax barriers or cylindrical lenticular lenses. Since its publication by Lippmann in 1908, the InI-based technique has been widely explored for both capturing the light fields of real scenes and for its use in eyewear-free auto-stereoscopic displays. It has been known for its limitations in low lateral and longitudinal resolutions, narrow depth of field (DOF), and narrow view angle. Compared with all other non-stereoscopic 3D display techniques, the simple optical architecture of an InI technique makes it attractive to integrate with HMD optical system and create a wearable light field display.

However, like other integral-imaging based display and imaging technologies, the current InI-based HMD method suffers from several major limitations: (1) narrow field of view (<30° diagonally); (2) low lateral resolution (about 10 arc minutes in the visual space); (3) low longitudinal resolution (about 0.5 diopters in the visual space); (4) narrow depth of field (DOF) (about 1 diopter for a 10-arc minute resolution criteria); (5) limited eyebox for crosstalk-free viewing(<5mm); and (6) limited resolution of viewing angle (>20 arc minutes per viewing). These limitations not only create significant barriers for adopting the technologies as high-performance solutions, but also potentially undermine the effectiveness of the technology for addressing the accommodation-convergence discrepancy problem.

Thus, the present disclosure details methods, design and embodiment of a high-performance head-mounted light field display based on integral imaging that overcomes some aspects of the performance limits of the state of the art summarized above.

## SUMMARY

In response to the challenges described above, in one of its aspects the present invention provides a high-performance HMD based on integral imaging that offers high lateral and longitudinal resolutions, large depth of field, cross-talk free eyebox, and increased viewing angle resolution. In this regard, the present invention may provide a head-mounted display integral imaging (InI) system, comprising a microscopic InI unit (micro-InI) configured to create light fields of a selected 3D scene at a selected position along an optical axis of the system, and a relay group having a vari-focal element (VFE) disposed therein. The relay group may be disposed on the optical axis at a location so the selected position is an optical conjugate of the relay group, the relay group configured to receive the light fields created by the microscopic InI unit and to create an intermediate 3D scene on the optical axis of the selected 3D scene. The relay group may be configured to tune the position along the optical axis of the intermediate 3D scene. In addition, eyepiece optics may be provided for imaging the intermediate 3D scene from the relay group into an exit pupil of the system for viewing by a user of the head-mounted display system. The microscopic InI unit (micro-InI) may be configured to reproduce full-parallax light fields of a 3D scene having a constrained viewing zone. A see-through unit may also be provided in optical communication with the eyepiece optics to transmit a view of a real world to the eyepiece optics for viewing by a user of the head-mounted display system. The VFE may be disposed at a position optically conjugate to the exit pupil. Further, the field of view of the system may be independent of the optical power of the VFE, and the VFE may be disposed on the optical axis at a location such that the compound optical power of the relay group is maintained constant, independent of the optical power of the VFE. Also, the relay group may be telecentric in object space or may be doubly telecentric. The eyepiece optics may include a wedge-shaped freeform prism. The diagonal field of view of the head-mounted display integral imaging (InI) system may be 35° and may have an optical resolution as high as 2 arc minutes per pixel.

## BRIEF DESCRIPTION OF THE DRAWINGS

The foregoing summary and the following detailed description of exemplary embodiments of the present invention may be further understood when read in conjunction with the appended drawings, in which:

Figure 1 schematically illustrates a conventional, monocular HMD in which an eyepiece magnifies the image rendered on a microdisplay and forms a virtual display appearing at a fixed, far distance from the eye;

Figure 2 schematically illustrates a near-eye light field display based on integral imaging;

Figure 3A schematically illustrates an exemplary configuration of a high-performance InI-based head-mounted light field display in accordance with the present invention;

Figure 3B schematically illustrates an exemplary configuration of a micro-InI unit in accordance with the present invention;

Figures 4A–4D schematically illustrate an exemplary configuration of a micro-InI unit in accordance with the present invention constructed to provide ray direction control by using: an aperture array (Fig. 4A), programmable spatial light modulator (Fig. 4B), a display source with controllable directional emissions engine (Fig. 4C); and a backlight source with a spatial light modulator as an exemplary controllable directional emissions engine (Fig. 4D);

Figure 5 schematically illustrates an exemplary configuration of a relay group in accordance with the present invention with a VFE (vari-focal element) placed at a position conjugate to the exit pupil of the eyepiece;

Figures 6A–6D schematically illustrate an exemplary configuration of an optical see-through InI-HMD design in accordance with the present invention using a freeform waveguide prism where part of the vari-focal relay group is incorporated into the eyepiece, with Fig.6A showing the display path layout, Fig. 6B showing the see-through view layout, Fig. 6C showing a segmented rear surface of the waveguide prism for extended see-through view, and Fig. 6D showing a front view of the rear surface of the waveguide prism;

Figures 7A, 7B schematically illustrate an exemplary configuration of 2D optical layout of an InI-HMD design configuration in accordance with the present invention, with Fig. 7A showing the light field display path and Fig. 7B the see-through path;

Figures 8A, 8B illustrate MTF (modulation transfer function) plots for the reconstruction central depth plane (CDP) depth of 3 diopters for fields on-axis (Fig. 8A) and for fields for the furthest MLA (micro lens array) element near the edge of the MLA (Fig. 8B);

Figures 9A, 9B illustrate MTF plots for the reconstruction CDP depth of 2 diopters for fields on-axis to the MLA (Fig. 9A) and fields for the furthest MLA element near the edge of the MLA (Fig. 9B);

Figures 10A, 10B illustrate MTF plots for the reconstruction CDP depth of 0 diopters for fields on-axis to the MLA (Fig. 10A) and for fields for the furthest MLA element near the edge of the MLA (Fig. 10B);

Figures 11A, 11B illustrate MTF plots for the reconstruction points shifted away from CDP by 0.25 diopters for fields on-axis to the MLA (Fig. 11A) and for fields for the furthest MLA element near the edge of the MLA (Fig. 11B);

Figures 12A, 12B illustrate MTF plots for the reconstruction points shifted away from CDP by 0.5 diopters for fields on-axis to the MLA (Fig. 12A) and for fields for the furthest MLA element near the edge of the MLA (Fig. 12B);

Figures 13A, 13B illustrate MTF plots for the reconstruction points shifted away from CDP by 0.75 diopters for fields on-axis to the MLA (Fig. 13A) and for fields for the furthest MLA element near the edge of the MLA (Fig. 13B);

Figures 14A, 14B illustrate MTF plots for the reconstruction points shifted away from CDP by 1 diopter for fields on-axis to the MLA (Fig. 14A) and for fields for the furthest MLA element near the edge of the MLA (Fig. 14B); and

Figure 15 illustrates the MTF for the see-through path FOV 65°x40°.

## DETAILED DESCRIPTION

Referring now to the figures, wherein like elements are numbered alike throughout, as shown in Fig. 3A, a HMD system 100 in accordance with the present invention may include three key subsystems: I) a microscopic InI unit (micro-InI) 130, II) a relay group 120 with a vari-focal element (VFE) 122 disposed therein for receiving the light fields from the InI unit 130, and III) eyepiece optics 110 for receiving the tuned intermediate 3D scene from the relay group 120. As illustrated in Fig. 3B, the micro-InI unit 130 can reproduce the full-parallax light fields of a 3D scene seen from a constrained viewing zone, where the full-parallax light fields offer the change of view perspectives of a 3D scene from both horizontal and vertical viewing directions. The constrained viewing zone optically corresponds to limiting the aperture of the micro-InI unit 130, and the constrained viewing zone is optically conjugate to the exit pupil of the display system 100 where a viewer's eye is placed to view the reconstructed 3D scene. The relay group 120 creates an intermediate image of the 3D scene reconstructed by the micro-InI unit 130 with a tunable position of its central depth plane (CDP). Depending on the magnification power of the eyepiece 110, the position of the CDP may be tunable in the range from about 0.5mm to as large

as hundreds of millimeters to create the perception of a 3D scene with a large depth range spanning from the optical infinity (0 diopter) to as close as 20cm (5 diopters). The relay group 120 may also facilitate the flip of the concavity of the reconstructed 3D scene AOB. The eyepiece optics 110 reimages the tunable 3D light fields into a viewer's eye and enlarges the tunable depth range of the 3D light fields into a large depth volume spacing from meters far to as close as a few centimeters. A see-through unit (not shown), which may be optics with a beamsplitter function, may optically communicate with the eyepiece optics 110 to optically enable non-obtrusive view of a real-world scene if a see-through view is desired. The micro-InI unit 130 of Fig. 3A, as further illustrated in Fig. 3B, may include a high-resolution microdisplay and a micro-lens array (MLA) 132. The focal length of the lenslets 133 in the MLA 132 is denoted as $f_{MLA}$ and the gap between the microdisplay 134 and the MLA 132 is noted as $g$. A set of 2D elemental images, each representing a different perspective of a 3D scene AOB, may be displayed on the high-resolution microdisplay 134. Through the MLA 132, each elemental image works as a spatially-incoherent object and the conical ray bundles emitted by the pixels in the elemental images intersect and integrally create the perception of a 3D scene that appears to emit light and occupy the 3D space. The central depth plane (CDP) of the reconstructed miniature scene, with a depth range of $z_0$, is located by the distance $l_{cdp}$ measured from the MLA 132. Such an InI system 130 allows the reconstruction of a 3D surface shape AOB with parallax information in both horizontal and vertical directions. The light field of the reconstructed 3D scene (*i.e.*, the curve AOB in Fig. 3B) may be optically coupled into eyepiece optics 110 via the relay group 120 for viewing by a user. In a resolution priority InI system ($f_{MLA} \neq g$), the central depth plane CDP of the reconstructed 3D scene is optically conjugate to the microdisplay 134 and its location is given by

$$l_{cdp} = gM_{MLA}, \tag{1}$$

Where $M_{MLA}$ is the magnification of the micro-InI unit 130, which may be expressed by

$$M_{MLA} = \frac{f_{MLA}}{g - f_{MLA}}. \tag{2}$$

As shown in Figs. 3A, 4A, optionally, an aperture array 136, including a group of ray-limiting apertures that matches the pitch of the MLA 132, may be inserted between the microdisplay 134 and MLA 132. The small aperture corresponding to each microlens 133 allows rays within the designed viewing window to propagate through the optics and reach the

eyebox while blocking unwanted rays from reaching an adjacent microlens 133 or while blocking rays from neighboring elemental images to reach a microlens 133. For instance, the black zone between the aperture A1 and A2 blocks the dashed rays originated from point P1 from reaching the MLA2 adjacent to the lenslet MLA1. These blocked rays are typically the main source of view cross-talk and ghost images observed in an InI display system. The distance from the microdisplay 134 to the aperture array 136 is denoted as $g_a$ and the diameter of aperture opening is denoted as $p_a$, which may be constrained by

$$g_a \leq g_{a-max} = g\frac{p_{ei}}{p_{ei}+p_{mla}}, \tag{3}$$

$$p_a \leq p_{a-max} = p_{ei}\frac{(g_{a-max}-g_a)}{g_{a-max}}, \tag{4}$$

Where $g_{a-max}$ and $p_{a-max}$ are the maximum allowable gap and aperture size, respectively, $p_{ei}$ is the dimension of the elemental image, and $p_{mla}$ is the pitch of the MLA 132.

One drawback in using an aperture array 136 with a fixed aperture size is that it can partially block rays for pixels located near the edge of each elemental images if the size of the elemental image changes. As illustrated in Figure 4A, a small part of the rays from point P1 which are supposed to propagate through lenslet MLA1 are blocked by the black zone between aperture A1 and aperture A2, causing vignetting-like effects such that viewer may observe reduction of image brightness for points near the edge of each elemental images. Figure 4B shows an alternative configuration to that of Fig. 4A in which the aperture array 136 is replaced by a programmable spatial light modulator (SLM) 135 so that the size and shape of each aperture can be dynamically adapted to avoid partially blocking desired rays. Figure 4C shows another embodiment of a micro-InI unit in accordance with the present invention in which the microdisplay 134 and aperture array 136 are replaced by a display source 131 with controllable directional emissions, where the light emission direction can be controlled precisely so that the rays from each pixel will only reach their corresponding MLA lenslet 133. Figure 4D demonstrates one possible configuration of such display source 131 where a spatial light modulator 135 is inserted between a backlight source 138 with non-direction emission and non-self-emissive microdisplay 137. The spatial light modulator 135 may be set to program and control the cone angle of the rays that illuminate the microdisplay 137 and reach the MLA 132.

A conventional InI-based display system can typically suffer from a limited depth of field (DOF) due to the rapid degradation of spatial resolution as the depths of 3D reconstruction points

shift away from that of the CDP. For instance, the 3D scene volume may need to be limited to less than 0.5 diopters in order to maintain a spatial resolution of 3 arc minutes or better in the visual space. In order to render a much larger 3D scene volume while maintaining a high spatial resolution, such as in the exemplary configuration of Fig. 3A, a relay group 120 with an electronically-controlled vari-focal element 122 sandwiched inside is inserted between the micro-InI 130 and the eyepiece 110. Exemplary VFE's 122 include liquid lenses, liquid crystal lenses, deformable mirrors, or any other tunable optical technology, such as electrically tunable optical technology. By dynamically controlling the optical power, $\varphi_R$, of the relay group 120 by applying different voltages to the VFE 122, the relay group 120 forms an intermediate image A'O'B' of the reconstructed miniature 3D scene created by the micro-InI 130. The central depth position CDP of the relayed intermediate scene is tunable axially (along the optical axis) with respect to the eyepiece 110. As a result, the depth volume of the magnified 3D virtual scene by the eyepiece 110 can be shifted axially from very close (e.g. 5 diopters) to very far (e.g. 0 diopter) while maintaining high lateral and longitudinal resolutions.

Figure 5 schematically illustrates an exemplary configuration of the vari-focal relay group 120, such as the relay group 120 of Fig. 3A, including a front lens group "Front Relay" 126 adjacent to the micro-InI unit 130, VFE optics 122 located in the middle functioning as the system stop, and rear lens group "Rear Relay" 124 adjacent to the eyepiece 110. The compound power, $\varphi_R$, of the relay group 120 is given by

$$\varphi_R = \varphi_1+\varphi_2 + \varphi_{vfe} - \varphi_1\varphi_2(t_1+t_2) - \varphi_{vfe}(\varphi_1 t_1 + \varphi_2 t_2) + \varphi_{vfe}\varphi_1\varphi_2 t_1 t_2 \quad (4)$$

Where $\varphi_1$, $\varphi_{VFE}$, and $\varphi_2$ are the optical power of the front lens group 126, VFE 122, and the rear lens group 124, respectively. $t_1$ and $t_2$ are the spaces between the front lens group 126 and VFE 122 and between the VFE 122 and the rear lens group 124. $z_0$ is the axial distance between the front lens group and the 3D scene reconstructed by the micro-InI unit 130. The axial position of the relayed intermediate scene is given by

$$z_0' = -\frac{1}{\frac{(1-z_0\varphi_1)-[z_0+(1-z_0\varphi_1)t_1]\varphi_{vfe}}{[z_0+(1-z_0\varphi_1)t_1]+\{(1-z_0\varphi_1)-[z_0+(1-z_0\varphi_1)t_1]\varphi_{vfe}\}t_2}-\varphi_2} \quad (5)$$

The lateral magnification of the vari-focal relay system is given by

$$M_R = \frac{1}{(1-z_0\varphi_1)-[z_0+(1-z_0\varphi_1)t_1]\varphi_{vfe}-\{[z_0+(1-z_0\varphi_1)t_1]+[(1-z_0\varphi_1)-[z_0+(1-z_0\varphi_1)t_1]\varphi_{vfe}]t_2\}\varphi_2} \quad (6)$$

Assuming $\varphi_e$ is the optical power of the eyepiece 110 and $Z_{RCDP}$ is the distance from the relayed CDP to the eyepiece 110, the apparent CDP position of the reconstructed 3D virtual scene through the eyepiece 110 is given by

$$z'_{RCDP} = \frac{1}{\varphi_e - \frac{1}{z_{RCDP}}} \quad (7)$$

The lateral magnification of the entire system through the eyepiece 110 is given by

$$M_t = \left| M_{MLA} \cdot M_R \cdot \frac{z'_{RCDP}}{z_{RCDP}} \right| \quad (8)$$

The field of view (FOV) of the entire system through the eyepiece 110 is given by, $FOV = 2\tan^{-1}\frac{h_0}{[h_{vfe}+(u_{vfe}-h_{vfe}\varphi_{vfe})t_1]+\{(u_{vfe}-h_{vfe}\varphi_{vfe})-[h_{vfe}+(u_{vfe}-h_{vfe}\varphi_{vfe})t_1]\varphi_1\}z_0}$ (9)

Where $t_3$ is the spacing between the eyepiece 110 and rear relay lens 124; $z_{xp}$ is the spacing between the exit pupil and the eyepiece 110; $h_0$ is the image height of the reconstructed scene, and we further define $u_{vfe} = [(1-z_{xp}\varphi_e)-(z_{xp}+(1-z_{xp}\varphi_e)t_3)\varphi_2]$, and $h_{vfe} = [(1-z_{xp}\varphi_e)-(z_{xp}+(1-z_{xp}\varphi_e)t_3)\varphi_2]-[(z_{xp}+(1-z_{xp}\varphi_e)t_3)\varphi_2+((1-z_{xp}\varphi_e)-(z_{xp}+(1-z_{xp}\varphi_e)t_3)\varphi_2)]t_2$.

When the VFE 122 is set to be an optical conjugate to the exit pupil of the eyepiece 110 ((i.e. $h_{vfe}=0$) where the entrance pupil of the eye is placed to view the display 134, we have $h_{vfe}=0$ and the FOV is independent of the optical power of the VFE 122. The equation in Eq. (9) is simplified into:

$$FOV = 2\tan^{-1}\frac{h_0}{u_{vfe}t_1+[u_{vfe}-u_{vfe}t_1\varphi_1]z_0} \quad (10)$$

As illustrated in Fig. 5, a preferred embodiment of the vari-focal relay group 120 is the placement of the VFE 122 at the back focal length of the front relay group 26 (i.e. $t_1=1/\varphi_1$) to make the VFE 122 an optical conjugate to the exit pupil of the eyepiece 110 ((i.e. $h_{vfe}=0$). With

this preferred embodiment, the compound power, $\varphi_R$, of the relay group 120 given by Eq. (4) is simplified into:

$$\varphi_R = \varphi_1 - \varphi_1\varphi_2 t_2 \tag{11}$$

The lateral magnification of the vari-focal relay system given by Eq. (6) is simplified into

$$M_R = \frac{1}{(1-z_0\varphi_R) - \frac{\varphi_{vfe}(1-\varphi_2 t_2)+\varphi_2(1+\varphi_1 t_2)}{\varphi_1}} \tag{12}$$

And so does the lateral magnification of the entire system given by Eq. (8).

When $t_1=1/\varphi_1$ and $h_{vfe}=0$, the FOV of the system is further simplified into

$$FOV = 2\tan^{-1}\frac{h_0\varphi_1}{u_{vfe}} \tag{13}$$

As demonstrated by Eqs. (10) through (13), the careful position of the VFE 122 in the preferred manner ensures that the compound optical power of the relay group 120 is maintained constant, independent of the optical power of the VFE 122 due to constant chief ray directions owing to the property of object-space telecentricity. As further demonstrated by Eq. (13), the subtended field angle of the display through the eyepiece 110 is further maintained constant, independent of the optical power of the VFE 122. Maintaining a constant optical power for the relay group 120 helps the virtually reconstructed 3D scene achieve constant field of view regardless of the focal depths of the CDP. Therefore a much larger volume of a 3D scene could be visually perceived without seams or artifacts in a gaze-contingent or time-multiplexing mode. It is worth noting that the lateral magnification of the relay group 120 given by Eq. (12) can be further maintained constant if $t_2=1/\varphi_2$ is satisfied, which makes the vari-focal relay group 120 a double-telecentric system.

The eyepiece 110 in Fig. 3A can take many different forms. For instance, to achieve a compact optical design of an optical see-through HMD, a wedge-shaped freeform prism can be adopted, through which the 3D scene reconstructed by the micro-InI unit 130 and relay group 120 is magnified and viewed. To enable see-through capability for AR systems, a freeform corrector lens with one of the surfaces coated with beamsplitter coating can be attached to the freeform prism eyepiece to correct the viewing axis deviation and undesirable aberrations introduced by the freeform prism to the real-world scene.

In another aspect of the present invention, part of the relay group 120 may be incorporated into the eyepiece optics 110, such as freeform eyepiece, such that the tunable intermediate 3D scene is formed inside the freeform eyepiece. In such a context, the eyepiece may be a wedge-shaped freeform waveguide prism, for example. Figure 6A schematically illustrates the concept of a freeform waveguide-like prism 850 formed by multiple freeform optical surfaces. The exit pupil is located where the use's eye is placed to view the magnified 3D scene. In the design, part of a traditional relay group 220 following the VFE 122 is incorporated into the prism 850 and fulfilled by the top portion 851 of the freeform waveguide prism 850 contained within the box labeled "Relay Group with VFE." A light ray emitted from a 3D point (e.g. A) is first refracted by a closest optical element 126 of the relay group 220 and transmitted into the prism 850, followed by a reflection by one or multiple freeform surfaces to create an intermediate image (e.g. A'). The axial position of the intermediate image (e.g. A') is tunable by the VFE 122. Multiple consecutive reflections by the subsequent surfaces and a final refraction through the exit surface 855allow the ray reaching the exit pupil of the system. Multiple bundles of rays from different elemental images may exist, but do so apparently from the same object point, each of which bundles represents a different view of the object, impinging on different locations of the exit pupil. These ray bundles integrally reconstruct a virtual 3D point (e.g. "A") located in front of the eye. Rather than requiring multiple optical elements, the optical path is naturally folded within a multi-surface prism 850, which helps reduce the overall volume and weight of the optics substantially when compared with designs using rotationally symmetric elements. Compared with a design using a traditional wedge-shaped 3-surface prism, the waveguide-like eyepiece design incorporates part of the relay function, enabling a much more compact system than combining a standalone relay group 120 with a 3-surface prism. Besides the advantage of compactness, the waveguide-like multi-fold eyepiece design offers a much more favorable form factor, because it enables the ability to fold the remaining relay group and micro-InI unit horizontally to the temple sides. The multiple folding not only yields a much more weight-balanced system, but also enables a substantially larger see-through FOV than using a wedge-shaped prism.

To enable see-through capability for AR systems, the bottom part 853 of the rear surface, marked as the eyepiece portion, of the prism 850 in Fig. 6A can be coated as a beamsplitting mirror, and a freeform corrector lens 840 including at least two freeform optical surfaces, may be

attached to the rear surface of the prism 850 to correct the viewing axis deviation and undesirable aberrations introduced by the freeform prism 850 to the real-world scene. The see-through schematic layout is shown in Fig. 6B. The rays from the virtual light field are reflected by the rear surface of the prism 850 while the rays from a real-world scene are transmitted through the freeform corrector lens 840 and prism 850. The front surface of the freeform corrector lens 840 matches the shape of the rear surface of the prism 850. The back surface of the freeform corrector lens 840 may be optimized to minimize the shift and distortion introduced to the rays from a real-world scene when the lens is combined with the prism 850. The additional corrector lens "compensator" does not noticeably increase the footprint and weight of the overall system.

In another aspect of the present invention, the bottom part 853 of the rear surface, marked as the eyepiece portion, of the prism 850 in Fig. 6A may be divided into two segments, the segment 853-1 and the segment 853-2. As schematically illustrated in Fig. 6C, the segment of 853-1 may be a reflective or partial reflective surface which receives the light fields generated by the micro-InI unit. A beamsplitting mirror coating on the segment of 853-1 also allows the transmission of the light rays from a real-world scene. The segment 853-2 is a transmissive or semi-transmissive surface which only receives the light rays from a real-world scene, while it does not receive the light fields generated by the micro-InI unit 130. Fig. 6D schematically illustrates a front view of the rear surface of the prism 850. The two surface segments, 853-1 and 853-2, intersect at an upper boundary of the aperture window required to receive the reconstructed 3D light fields by the micro-InI unit 130, and they may be made by two separate freeform surfaces. The division of the bottom part of the rear surface 853 into two separate segments 853-1, 853-2 with different light paths provides the ability to substantially enlarge the FOV of the see-through view beyond the FOV of the display path without being subject to the constraints of the virtual display path. As shown in Fig. 6C, a freeform corrector lens 840 may be attached to the rear surface of the prism 850 to correct the viewing axis deviation and undesirable aberrations introduced by the freeform prism 850 to the real-world scene. The rays from the virtual light field are reflected by the segment 853-1 of the rear surface of the prism 850 while the rays from a real-world scene are transmitted through both the segments 853-1 and 853-2 of the prism 850 and the freeform corrector lens 840. The surface segment 853-2 may be optimized to minimize visual artifacts of see-through view when it is combined with the freeform corrector lens 840. The front surface of the freeform corrector lens 840 matches the shape of the surface segments 853-1 and 853-2 of

the prism 850. The back surface of the freeform corrector lens 840 may be optimized to minimize the shift and distortion introduced to the rays from a real-world scene when the freeform corrector lens 840 is combined with the prism 850.

In accordance with yet another aspect of the present invention, Figure 7A schematically illustrates an optical design of a physical system that embodies the conceptual system of Fig. 6A. Figure 7A illustrates the 2D optical layout of the light field display path, and Fig. 7B shows the optical layout of the see-through path. The optical system of the light field display includes a micro-InI unit, a relay group with VFE, and a freeform waveguide. A part of the relay group may be incorporated into the waveguide. The Micro-InI unit may include a microdisplay S0, a pinhole array S1, and a microlens array S2. The relay group may include four lenses, a commercially available VFE (Electrical Lens EL 10-30 by Optotune Inc.), and two freeform surfaces (Surface S19 and S20). The freeform waveguide prism 900 may be formed by multiple freeform optical surfaces which are labeled as S19, S20, S21, and S22, respectively. In the design, part of a traditional relay group following the VFE may be incorporated into the prism 900 and fulfilled by the Surface S19 and S20. A light ray emitted from a 3D point (e.g. A) is first refracted by the surface S19 of the prism 900, followed by a reflection by the surface S20 to create an intermediate image (e.g. A'). The axial position of the intermediate image (e.g. A') is tunable by the VFE. Two more consecutive reflections by the surfaces S21' and S22-1 and a final refraction through the surface S21 allow the ray to reach the exit pupil of the system. There exist multiple bundles of rays from different elemental images but apparently from the same object point, each of which represents a different view of the object, impinging on different locations of the exit pupil. These ray bundles integrally reconstruct a virtual 3D point located in front of the eye. The rays reflected by the Surface S21' of the waveguide are required to satisfy the condition of total internal reflection. The rear surfaces S22-1, S22-2 of the prism 900 may be coated with a mirror coating for building an immersive HMD system which blocks the view of the real-world scene. Alternatively, the surface S22-1 may be coated with a beamsplitting coating if optical see-through capability is desired using the auxiliary lens, as shown in Fig. 7B.

It should be noted that in the design disclosed hereby the Z-axis is along the viewing direction, the Y-axis is parallel to the horizontal direction aligning with interpupilary direction, and the X-axis is in the vertical direction aligning with the head orientation. As a result, the overall waveguide system is symmetric about the horizontal (YOZ) plane, and the optical

surfaces (S19, S20, S21, and S22) are decentered along the horizontal Y-axis and rotated about the vertical X-axis. The optical path is folded in the horizontal YOZ plane. This arrangement allows the micro-InI unit and the vari-focal relay group to be mounted on the temple side of the user's head, resulting in a balanced and ergonomic system packaging.

Table 1 highlighted some of the key performance specifications for the system of Fig. 7A. The system offers the ability to render the true 3D light field of a 3D scene which subtends a diagonal FOV of 35° and achieves an optical resolution as high as 2 arc minutes per pixel in the visual space. Furthermore, the system offers a large depth range, tunable from 0 to 5 diopters, with a high longitudinal resolution of about 0.1 diopters for a monocular display. Moreover, the system achieves a high view density of about 0.5/mm$^2$, where the view density, σ, is defined as the number of unique views per unit area on the exit pupil, given by:

$$\sigma = \frac{N}{A_{XP}}$$

where N is the total number of views and $A_{XP}$ is the area of the exit pupil of the display system. A view density of 0.5/mm$^2$ is equivalent to a viewing angle resolution of approximately 1 arc minute for objects at distance of 0.2 diopters. The exit pupil diameter for crosstalk-free viewing, also known as the eyebox of the display, is about 6mm. In this embodiment, the exit pupil diameter is limited by the aperture size of the commercial VFE and it can be increased if another larger-aperture VFE is adopted. Finally, the system offers a large see-through FOV, greater than 65° horizontally and 40° vertically. The microdisplay utilized in our prototype is a 0.7" organic light emitting display (OLED) with an 8μm color pixel and pixel resolution of 1920x1080 (ECX335A by Sony). The optics design itself, however, is able to support OLED panels of different dimensions or other type of microdisplays such as liquid crystal displays that have a color pixel size greater than 6 μm.

**Table 1—First-order system specifications**

| | |
|---|---|
| Tunable depth range of central depth plane (CDP) | *0 ~ 5 diopters* |
| Field of view (Virtual Display) | *35° (diagonal), or 30.5° (Horizontal) x 17.5° (Vertical) at CDP* |
| Field of view (See-through) | *>75° (diagonal), or >65° (Horizontal) x 40° (Vertical)* |

| | |
|---|---|
| Focal length of front relay group | 24 mm |
| Focal length of rear relay group | 24 mm |
| Focal range of the tunable lens | 75-100mm (8.5 diopters) |
| Eyepiece focal length, $f_{eye}$ | 27.5 mm |
| Exit pupil diameter | 6 mm |
| Pitch of the lenslet in MLA | 1 mm |
| F-number of the MLA | 3.3 |

An exemplary implementation of the system of Fig. 7A is provided, Tables 2 through 5, in form of the optical surface data. Table 2 summarizes the basic parameters of the display path (units: mm). Tables 3 through 5 provide the optimized coefficients defining the non-spherical optical surfaces.

**Table 2—Optical specifications of the InI-HMD display path**

| Element number or name | Surface No. | Surface Type | Y Radius | Thickness | Material | Refract Mode |
|---|---|---|---|---|---|---|
| Aperture | | Sphere | Infinity | 2.215 | | Refract |
| MLA | S1 | Asphere | -5.32 | 3 | PMMA | Refract |
| | S2 | Asphere | -1.48 | 13.833 | | Refract |
| | S3 | Sphere | Infinity | 10.547 | | Refract |
| Front relay group | S4 | Sphere | 35.09 | 6.6 | NBK7_SCHOTT | Refract |
| | S5 | Sphere | -35.09 | 9.970 | | Refract |
| | S6 | Sphere | 12.92 | 4.3 | NBK7_SCHOTT | Refract |
| | S7 | Sphere | Infinity | 2.457 | | Refract |
| | S8 | Sphere | -39.78 | 2.5 | NSF11_SCHOTT | Refract |
| | S9 | Sphere | 39.78 | 1.75 | | Refract |
| VFE | S10 | Sphere | Infinity | 1.15 | | Refract |
| | S11 | Sphere | Infinity | 0.5 | BK7_SCHOTT | Refract |
| | S12 | Sphere | Infinity | 2.758 | 'OL1024' | Refract |
| | S13 | Sphere | -28.5714 | 4.492 | | Refract |
| | S14 | Sphere | Infinity | 0.5 | BK7_SCHOTT | Refract |

| | | | | | | | |
|---|---|---|---|---|---|---|---|
| | | S15 | Sphere | Infinity | 1.15 | | Refract |
| | | S16 | Sphere | Infinity | 1 | | Refract |
| Lens | | S17 | Sphere | 40.67 | 5.3 | NBK7_SCHOTT | Refract |
| | | S18 | Sphere | -40.67 | 0 | | Refract |
| Waveguide | | S19 | XY Polynomial | 31.04167 | 0 | PMMA | Refract |
| | | S20 | XY Polynomial | -54.2094 | 0 | PMMA | Reflect |
| | | S21 | XY Polynomial | -145.276 | 0 | PMMA | Reflect |
| | | S22 | XY Polynomial | -47.3572 | 0 | PMMA | Reflect |
| | | S21' | XY Polynomial | -145.276 | 0 | | Refract |
| | | | | | | | |

A high resolution microdisplay with pixels as small as 6μm is adopted to achieve a high resolution virtual reconstructed 3D image. To achieve such high-resolution imaging for the micro-InI unit, a microlens array (MLA) formed by aspherical surfaces may specifically be designed. Each of the aspherical surfaces of the MLA may be described as,

$$z = \frac{cr^2}{1+\sqrt{1-(1+k)c^2r^2}} + Ar^4 + Br^6 + Cr^8 + Dr^{10} + Er^{12}, \quad (14)$$

where z is the sag of the surface measured along the z-axis of a local x, y, z coordinate system, c is the vertex curvature, r is the radial distance, k is the conic constant, A through E are the 4th, 6th, 8th, 10th and 12th order deformation coefficients, respectively. The material of the MLA is PMMA. Table 3 provides the coefficients for the surfaces S1 and S2.

**Table 3—Aspherical surface definitions for microlens array (MLA)**

| | S1 | S2 |
|---|---|---|
| Y Radius | -5.32 | -1.48 |

| | | |
|---|---|---|
| Conic Constant (K) | 30 | -0.809 |
| 4th Order Coefficient (A) | -0.157 | -0.013 |
| 6th Order Coefficient (B) | -0.092 | 0.002 |

To enable enlarged see-through FOV, the freeform waveguide prism 900 may be formed by five freeform surfaces, labeled as surface S19, S20, S21/S21', S22-1, and S22-2, respectively. The freeform corrector lens may be formed by two freeform surfaces, in which the front surface shares the same surface specifications as the surfaces S22-1 and S22-2 of the waveguide prism 900 and the rear surface is denoted as surface S23. The surface segment of S22-1 is a reflective or partial reflective surface which receives the light fields generated by the micro-InI unit. A beamsplitting mirror coating on the segment of S22-1 also allows the transmission of the light rays from a real-world scene for see-through capability. The surface segment S22-2 is a transmissive or semi-transmissive surface which only receives the light rays from a real-world scene, while it does not receive the light fields generated by the micro-InI unit.

The freeform surfaces, including S19, S20, S21/S21', S22-1, and S23 may be described mathematically as

$$z=\frac{cr^2}{1+\sqrt{1-(1+k)c^2r^2}}+\sum_{j=2}^{66}C_j x^m y^n \qquad j=\frac{(m+n)^2+m+3n}{2}+1, \quad (15)$$

where z is the sag of the free-form surface measured along the z-axis of a local x, y, z coordinate system, c is the vertex curvature (CUY), r is the radial distance, k is the conic constant, and $C_j$ is the coefficient for $x^m y^n$. The material for both the waveguide prism and compensation lens is PMMA. Tables 4 through 8 provide the coefficients for the surfaces S19 through S21, S22-1, and S23, respectively, and Table 9 provides the surface references of each optical surface.

During the design process, the specifications for the Surface segment S22-1 were obtained after the optimization of the light field display path through the prism 900 composed of the micro-InI unit, the relay lens group, and the surfaces S19. S20, S21/21', and S22-1. The required aperture dimensions of Surfaces S20 and S22-1 were determined first for the light field display path. Then Surfaces S20, S21 and S22-1 were imported into 3D modeling software such as Solidworks® from which the Surface S22-2 was created. The shape of the Surface S22-2 was

created in the modeling software by satisfying the following requirements: (1) it intersects with Surface S22-1 along or above the upper boundary line of the required aperture for surface S22-1 defined by the display path; (2) along the intersection line between the surface S22-2 and S22-2, the surface slopes at the intersection points on the surface S22-2 approximately match, if not equal, with those corresponding points on the surface S22-1 to ensure the two surfaces to appear to be nearly continuous, which minimizes visual artifacts to the see-through view when it is combined with a matching freeform corrector lens; (3) the Surface S22-2 intersects with the surface S20 along or below the lower boundary line of the required aperture for surface S20, defined by the display path; and (4) the overall thickness between the surface S21 and S22-2 is minimized. Finally, a freeform shape of the Surface S22-2 is obtained in the 3D modeling software which is combined with the surfaces S19, S20, S21/21', and S22-1 to create an enclosed freeform waveguide prism. Fig. 7B demonstrated a substantially enlarged see-through FOV through the method described above.

**Table 4—Surface definition for freeform surface S19**

| | |
|---|---|
| Y Radius | 31.0417 |
| Y Curvature | 3.2215e-2 |
| Conic Constant (SCO K \| C1) | -30 |
| X (SCO X \| C2) | 0 |
| Y (SCO Y \| C3) | 0 |
| X**2 (SCO X2 \| C4) | -0.0181749 |
| X * Y (SCO XY \| C5) | 0 |
| Y**2 (SCO Y2 \| C6) | -0.03201 |
| X**3 (SCO Y3 \| C7) | 0 |
| X**2 * Y (SCO X2Y \| C8) | -0.002337 |
| X Y**2 (SCO XY2 \| C9) | 0 |
| Y**3 (SCO Y3 \| C10) | -0.00340584 |
| X**4 (SCO X4 \| C11) | 2.214179429e-005 |
| X**3 * Y (SCO X3Y \| C12) | 0 |
| X**2 * Y**2 (SCO X2Y2 \| C13) | -8.34173481e-005 |

| | |
|---|---|
| X * Y**3 (SCO XY3 \| C14) | 0 |
| Y**4 (SCO Y4 \| C15) | -0.00012019 |
| X**5 (SCO X5 \| C16) | 0 |
| X**4 * Y (SCO X4Y \| C17) | -1.9551358e-006 |
| X**3 * Y**2 (SCO X3Y2 \| C18) | 0 |
| X**2 * Y**3 (SCO X2Y3 \| C19) | -5.7523828e-007 |
| X * Y**4 (SCO XY4 \| C20) | 0 |
| Y**5 (SCO Y5 \| C21) | -2.18978576e-006 |
| X**6 (SCO X6 \| C22) | -1.08276112e-007 |
| X**5 * Y (SCO X5Y \| C23) | 0 |
| X**4 * Y**2 (SCO X4Y2 \| C24) | -3.584137e-007 |
| X**3 * Y**3 (SCO X3Y3 \| C25) | 0 |
| X**2 * Y**4 (SCO X2Y4 \| C26) | 9.1214167e-008 |
| X * Y**5 (SCO XY5 \| C27) | 0 |
| Y**6 (SCO Y6 \| C28) | -5.28011679e-009 |
| X**7 (SCO X7 \| C29) | 0 |
| X**6 * Y (SCO X6Y \| C30) | 0 |
| X**5 * Y**2 (SCO X5Y2 \| C31) | 0 |
| X**4 * Y**3 (SCO X4Y3 \| C32) | 0 |
| X**3 * Y**4 (SCO X3Y4 \| C33) | 0 |
| X**2 * Y**5 (SCO S2Y5 \| C34) | 0 |
| X * Y**6 (SCO XY6 \| C35) | 0 |
| Y**7 (SCO Y7 \| C36) | 0 |
| X**8 (SCO X8 \| C37) | 0 |
| X**7 * Y (SCO X7Y \| C38) | 0 |
| X**6 * Y**2 (SCO X6Y2 \| C39) | 0 |
| X**5 * Y**3 (SCO X5Y3 \| C40) | 0 |
| X**4 * Y**4 (SCO X4Y4 \| C41) | 0 |
| X**3 * Y**5 (SCO X3Y5 \| C42) | 0 |

| | |
|---|---|
| X**2 * Y**6 (SCO X2Y6 \| C43) | 0 |
| X * Y**7 (SCO XY7 \| C44) | 0 |
| Y**8 (SCO Y8 \| C45) | 0 |
| X**9 (SCO X9 \| C46) | 0 |
| X**8 * Y (SCO X8Y \| C47) | 0 |
| X**7 * Y**2 (SCO X7Y2 \| C48) | 0 |
| X**6 * Y**3 (SCO X6Y3 \| C49) | 0 |
| X**5 * Y**4 (SCO X5Y4 \| C50) | 0 |
| X**4 * Y**5 (SCO X4Y5 \| C51) | 0 |
| X**3 * Y**6 (SCO X3Y6 \| C52) | 0 |
| X**2 * Y**7 (SCO X2Y7 \| C53) | 0 |
| X * Y**8 (SCO XY8 \| C54) | 0 |
| Y**9 (SCO Y9 \| C55) | 0 |
| X**10 (SCO X10 \| C56) | 0 |
| X**9 * Y (SCO X9Y \| C57) | 0 |
| X**8 * Y**2 (SCO X8Y2 \| C58) | 0 |
| X**7 * Y**3 (SCO X7Y3 \| C59) | 0 |
| X**6 * Y**4 (SCO X6Y4 \| C60) | 0 |
| X**5 * Y**5 (SCO X5Y5 \| C61) | 0 |
| X**4 * Y**6 (SCO X4Y6 \| C62) | 0 |
| X**3 * Y**7 (SCO X3Y7 \| C63) | 0 |
| X**2 * Y**8 (SCO X2Y8 \| C64) | 0 |
| X * Y**9 (SCO XY9 \| C65) | 0 |
| Y**10 (SCO Y10 \| C66) | 0 |

**Table 5—Surface definition for freeform surface S20**

| | |
|---|---|
| Y Radius | -54.2094 |
| Y Curvature | -1.845e-2 |
| Conic Constant (SCO K \| C1) | -13.0997 |

| | |
|---|---|
| X (SCO X \| C2) | 0 |
| Y (SCO Y \| C3) | 0 |
| X**2 (SCO X2 \| C4) | 0.0011699 |
| X * Y (SCO XY \| C5) | 0 |
| Y**2 (SCO Y2 \| C6) | 0.00676927 |
| X**3 (SCO Y3 \| C7) | 0 |
| X**2 * Y (SCO X2Y \| C8) | -4.52710486e-005 |
| X Y**2 (SCO XY2 \| C9) | 0 |
| Y**3 (SCO Y3 \| C10) | -0.00011081 |
| X**4 (SCO X4 \| C11) | -1.1510996e-005 |
| X**3 * Y (SCO X3Y \| C12) | 0 |
| X**2 * Y**2 (SCO X2Y2 \| C13) | -9.13752747e-006 |
| X * Y**3 (SCO XY3 \| C14) | 0 |
| Y**4 (SCO Y4 \| C15) | -5.5289301e-006 |
| X**5 (SCO X5 \| C16) | 0 |
| X**4 * Y (SCO X4Y \| C17) | -8.8179807e-007 |
| X**3 * Y**2 (SCO X3Y2 \| C18) | 0 |
| X**2 * Y**3 (SCO X2Y3 \| C19) | -1.06187669e-006 |
| X * Y**4 (SCO XY4 \| C20) | 0 |
| Y**5 (SCO Y5 \| C21) | -3.38263553e-007 |
| X**6 (SCO X6 \| C22) | 4.77710263e-008 |
| X**5 * Y (SCO X5Y \| C23) | 0 |
| X**4 * Y**2 (SCO X4Y2 \| C24) | 6.21915481e-008 |
| X**3 * Y**3 (SCO X3Y3 \| C25) | 0 |
| X**2 * Y**4 (SCO X2Y4 \| C26) | 1.43552488e-007 |
| X * Y**5 (SCO XY5 \| C27) | 0 |
| Y**6 (SCO Y6 \| C28) | 5.362211474e-008 |
| X**7 (SCO X7 \| C29) | 0 |
| X**6 * Y (SCO X6Y \| C30) | 1.193262499e-008 |

| | |
|---|---|
| X**5 * Y**2 (SCO X5Y2 \| C31) | 0 |
| X**4 * Y**3 (SCO X4Y3 \| C32) | -6.01716948e-009 |
| X**3 * Y**4 (SCO X3Y4 \| C33) | 0 |
| X**2 * Y**5 (SCO S2Y5 \| C34) | -8.19603928e-009 |
| X * Y**6 (SCO XY6 \| C35) | 0 |
| Y**7 (SCO Y7 \| C36) | -2.505270966e-009 |
| X**8 (SCO X8 \| C37) | -8.149026e-010 |
| X**7 * Y (SCO X7Y \| C38) | 0 |
| X**6 * Y**2 (SCO X6Y2 \| C39) | -1.84757517e-010 |
| X**5 * Y**3 (SCO X5Y3 \| C40) | 0 |
| X**4 * Y**4 (SCO X4Y4 \| C41) | 2.388128888e-010 |
| X**3 * Y**5 (SCO X3Y5 \| C42) | 0 |
| X**2 * Y**6 (SCO X2Y6 \| C43) | 1.61835037e-010 |
| X * Y**7 (SCO XY7 \| C44) | 0 |
| Y**8 (SCO Y8 \| C45) | 3.966177607e-011 |
| X**9 (SCO X9 \| C46) | 0 |
| X**8 * Y (SCO X8Y \| C47) | 0 |
| X**7 * Y**2 (SCO X7Y2 \| C48) | 0 |
| X**6 * Y**3 (SCO X6Y3 \| C49) | 0 |
| X**5 * Y**4 (SCO X5Y4 \| C50) | 0 |
| X**4 * Y**5 (SCO X4Y5 \| C51) | 0 |
| X**3 * Y**6 (SCO X3Y6 \| C52) | 0 |
| X**2 * Y**7 (SCO X2Y7 \| C53) | 0 |
| X * Y**8 (SCO XY8 \| C54) | 0 |
| Y**9 (SCO Y9 \| C55) | 0 |
| X**10 (SCO X10 \| C56) | 0 |
| X**9 * Y (SCO X9Y \| C57) | 0 |
| X**8 * Y**2 (SCO X8Y2 \| C58) | 0 |
| X**7 * Y**3 (SCO X7Y3 \| C59) | 0 |

| | |
|---|---|
| X**6 * Y**4 (SCO X6Y4 \| C60) | 0 |
| X**5 * Y**5 (SCO X5Y5 \| C61) | 0 |
| X**4 * Y**6 (SCO X4Y6 \| C62) | 0 |
| X**3 * Y**7 (SCO X3Y7 \| C63) | 0 |
| X**2 * Y**8 (SCO X2Y8 \| C64) | 0 |
| X * Y**9 (SCO XY9 \| C65) | 0 |
| Y**10 (SCO Y10 \| C66) | 0 |

**Table 6—Surface definition for freeform surface S21/S21'**

| | |
|---|---|
| Y Radius | -145.276 |
| Y Curvature | -6.88e-3 |
| Conic Constant (SCO K \| C1) | -1.5654 |
| X (SCO X \| C2) | 0 |
| Y (SCO Y \| C3) | 0 |
| X**2 (SCO X2 \| C4) | -0.0142277 |
| X * Y (SCO XY \| C5) | 0 |
| Y**2 (SCO Y2 \| C6) | 0.00392684 |
| X**3 (SCO Y3 \| C7) | 0 |
| X**2 * Y (SCO X2Y \| C8) | 0.000646111 |
| X Y**2 (SCO XY2 \| C9) | 0 |
| Y**3 (SCO Y3 \| C10) | 2.44041e-005 |
| X**4 (SCO X4 \| C11) | 0.000151 |
| X**3 * Y (SCO X3Y \| C12) | 0 |
| X**2 * Y**2 (SCO X2Y2 \| C13) | -8.2192e-006 |
| X * Y**3 (SCO XY3 \| C14) | 0 |
| Y**4 (SCO Y4 \| C15) | -3.028061e-007 |
| X**5 (SCO X5 \| C16) | 0 |
| X**4 * Y (SCO X4Y \| C17) | -4.13244e-006 |
| X**3 * Y**2 (SCO X3Y2 \| C18) | 0 |

| | |
|---|---|
| X**2 * Y**3 (SCO X2Y3 \| C19) | 2.964542e-008 |
| X * Y**4 (SCO XY4 \| C20) | 0 |
| Y**5 (SCO Y5 \| C21) | 1.127521e-009 |
| X**6 (SCO X6 \| C22) | 4.4371187e-008 |
| X**5 * Y (SCO X5Y \| C23) | 0 |
| X**4 * Y**2 (SCO X4Y2 \| C24) | 2.7676459e-008 |
| X**3 * Y**3 (SCO X3Y3 \| C25) | 0 |
| X**2 * Y**4 (SCO X2Y4 \| C26) | -3.277381e-011 |
| X * Y**5 (SCO XY5 \| C27) | 0 |
| Y**6 (SCO Y6 \| C28) | -1.4480674e-012 |
| X**7 (SCO X7 \| C29) | 0 |
| X**6 * Y (SCO X6Y \| C30) | 0 |
| X**5 * Y**2 (SCO X5Y2 \| C31) | 0 |
| X**4 * Y**3 (SCO X4Y3 \| C32) | 0 |
| X**3 * Y**4 (SCO X3Y4 \| C33) | 0 |
| X**2 * Y**5 (SCO S2Y5 \| C34) | 0 |
| X * Y**6 (SCO XY6 \| C35) | 0 |
| Y**7 (SCO Y7 \| C36) | 0 |
| X**8 (SCO X8 \| C37) | 0 |
| X**7 * Y (SCO X7Y \| C38) | 0 |
| X**6 * Y**2 (SCO X6Y2 \| C39) | 0 |
| X**5 * Y**3 (SCO X5Y3 \| C40) | 0 |
| X**4 * Y**4 (SCO X4Y4 \| C41) | 0 |
| X**3 * Y**5 (SCO X3Y5 \| C42) | 0 |
| X**2 * Y**6 (SCO X2Y6 \| C43) | 0 |
| X * Y**7 (SCO XY7 \| C44) | 0 |
| Y**8 (SCO Y8 \| C45) | 0 |
| X**9 (SCO X9 \| C46) | 0 |
| X**8 * Y (SCO X8Y \| C47) | 0 |

| | |
|---|---|
| X**7 * Y**2 (SCO X7Y2 \| C48) | 0 |
| X**6 * Y**3 (SCO X6Y3 \| C49) | 0 |
| X**5 * Y**4 (SCO X5Y4 \| C50) | 0 |
| X**4 * Y**5 (SCO X4Y5 \| C51) | 0 |
| X**3 * Y**6 (SCO X3Y6 \| C52) | 0 |
| X**2 * Y**7 (SCO X2Y7 \| C53) | 0 |
| X * Y**8 (SCO XY8 \| C54) | 0 |
| Y**9 (SCO Y9 \| C55) | 0 |
| X**10 (SCO X10 \| C56) | 0 |
| X**9 * Y (SCO X9Y \| C57) | 0 |
| X**8 * Y**2 (SCO X8Y2 \| C58) | 0 |
| X**7 * Y**3 (SCO X7Y3 \| C59) | 0 |
| X**6 * Y**4 (SCO X6Y4 \| C60) | 0 |
| X**5 * Y**5 (SCO X5Y5 \| C61) | 0 |
| X**4 * Y**6 (SCO X4Y6 \| C62) | 0 |
| X**3 * Y**7 (SCO X3Y7 \| C63) | 0 |
| X**2 * Y**8 (SCO X2Y8 \| C64) | 0 |
| X * Y**9 (SCO XY9 \| C65) | 0 |
| Y**10 (SCO Y10 \| C66) | 0 |

**Table 7—Surface definition for freeform surface S22-1**

| | |
|---|---|
| Y Radius | -47.3572012741099 |
| Y Curvature | -2.111611e-2 |
| Conic Constant (SCO K \| C1) | -4.32135 |
| X (SCO X \| C2) | 0 |
| Y (SCO Y \| C3) | 0 |
| X**2 (SCO X2 \| C4) | 0.000908 |
| X * Y (SCO XY \| C5) | 0 |
| Y**2 (SCO Y2 \| C6) | 0.005975 |

| | |
|---|---|
| X**3 (SCO Y3 \| C7) | 0 |
| X**2 * Y (SCO X2Y \| C8) | 4.66442802e-005 |
| X Y**2 (SCO XY2 \| C9) | 0 |
| Y**3 (SCO Y3 \| C10) | 0.000101981 |
| X**4 (SCO X4 \| C11) | -5.17499005e-006 |
| X**3 * Y (SCO X3Y \| C12) | 0 |
| X**2 * Y**2 (SCO X2Y2 \| C13) | -4.7451096e-006 |
| X * Y**3 (SCO XY3 \| C14) | 0 |
| Y**4 (SCO Y4 \| C15) | -2.4419368e-007 |
| X**5 (SCO X5 \| C16) | 0 |
| X**4 * Y (SCO X4Y \| C17) | -1.9769907e-007 |
| X**3 * Y**2 (SCO X3Y2 \| C18) | 0 |
| X**2 * Y**3 (SCO X2Y3 \| C19) | 3.352610999e-008 |
| X * Y**4 (SCO XY4 \| C20) | 0 |
| Y**5 (SCO Y5 \| C21) | 1.61592149e-008 |
| X**6 (SCO X6 \| C22) | 8.08067957e-009 |
| X**5 * Y (SCO X5Y \| C23) | 0 |
| X**4 * Y**2 (SCO X4Y2 \| C24) | 7.3374791e-009 |
| X**3 * Y**3 (SCO X3Y3 \| C25) | 0 |
| X**2 * Y**4 (SCO X2Y4 \| C26) | 6.611479e-009 |
| X * Y**5 (SCO XY5 \| C27) | 0 |
| Y**6 (SCO Y6 \| C28) | 9.4341645e-011 |
| X**7 (SCO X7 \| C29) | 0 |
| X**6 * Y (SCO X6Y \| C30) | 7.9369652e-010 |
| X**5 * Y**2 (SCO X5Y2 \| C31) | 0 |
| X**4 * Y**3 (SCO X4Y3 \| C32) | 6.27173598e-010 |
| X**3 * Y**4 (SCO X3Y4 \| C33) | 0 |
| X**2 * Y**5 (SCO S2Y5 \| C34) | 1.332732e-010 |
| X * Y**6 (SCO XY6 \| C35) | 0 |

| | |
|---|---|
| Y**7 (SCO Y7 \| C36) | -1.5647943e-011 |
| X**8 (SCO X8 \| C37) | -2.12470728e-012 |
| X**7 * Y (SCO X7Y \| C38) | 0 |
| X**6 * Y**2 (SCO X6Y2 \| C39) | 3.27745944e-011 |
| X**5 * Y**3 (SCO X5Y3 \| C40) | 0 |
| X**4 * Y**4 (SCO X4Y4 \| C41) | 1.07463864e-011 |
| X**3 * Y**5 (SCO X3Y5 \| C42) | 0 |
| X**2 * Y**6 (SCO X2Y6 \| C43) | 1.347790032e-012 |
| X * Y**7 (SCO XY7 \| C44) | 0 |
| Y**8 (SCO Y8 \| C45) | -9.599201503e-014 |
| X**9 (SCO X9 \| C46) | 0 |
| X**8 * Y (SCO X8Y \| C47) | 0 |
| X**7 * Y**2 (SCO X7Y2 \| C48) | 0 |
| X**6 * Y**3 (SCO X6Y3 \| C49) | 0 |
| X**5 * Y**4 (SCO X5Y4 \| C50) | 0 |
| X**4 * Y**5 (SCO X4Y5 \| C51) | 0 |
| X**3 * Y**6 (SCO X3Y6 \| C52) | 0 |
| X**2 * Y**7 (SCO X2Y7 \| C53) | 0 |
| X * Y**8 (SCO XY8 \| C54) | 0 |
| Y**9 (SCO Y9 \| C55) | 0 |
| X**10 (SCO X10 \| C56) | 0 |
| X**9 * Y (SCO X9Y \| C57) | 0 |
| X**8 * Y**2 (SCO X8Y2 \| C58) | 0 |
| X**7 * Y**3 (SCO X7Y3 \| C59) | 0 |
| X**6 * Y**4 (SCO X6Y4 \| C60) | 0 |
| X**5 * Y**5 (SCO X5Y5 \| C61) | 0 |
| X**4 * Y**6 (SCO X4Y6 \| C62) | 0 |
| X**3 * Y**7 (SCO X3Y7 \| C63) | 0 |
| X**2 * Y**8 (SCO X2Y8 \| C64) | 0 |

| | |
|---|---|
| X * Y**9 (SCO XY9 \| C65) | 0 |
| Y**10 (SCO Y10 \| C66) | 0 |

**Table 8—Surface definition for freeform surface S23**

| | |
|---|---|
| Y Radius | 149.3605 |
| Y Curvature | 6.695e-3 |
| Conic Constant (SCO K \| C1) | 9.81433 |
| X (SCO X \| C2) | 0 |
| Y (SCO Y \| C3) | 0 |
| X**2 (SCO X2 \| C4) | -0.024663 |
| X * Y (SCO XY \| C5) | 0 |
| Y**2 (SCO Y2 \| C6) | 0.0612683 |
| X**3 (SCO Y3 \| C7) | 0 |
| X**2 * Y (SCO X2Y \| C8) | 0.0010723 |
| X Y**2 (SCO XY2 \| C9) | 0 |
| Y**3 (SCO Y3 \| C10) | 2.4386556e-005 |
| X**4 (SCO X4 \| C11) | 0.00013098 |
| X**3 * Y (SCO X3Y \| C12) | 0 |
| X**2 * Y**2 (SCO X2Y2 \| C13) | -1.2892527e-006 |
| X * Y**3 (SCO XY3 \| C14) | 0 |
| Y**4 (SCO Y4 \| C15) | 2.62995523e-006 |
| X**5 (SCO X5 \| C16) | 0 |
| X**4 * Y (SCO X4Y \| C17) | -6.0819504e-006 |
| X**3 * Y**2 (SCO X3Y2 \| C18) | 0 |
| X**2 * Y**3 (SCO X2Y3 \| C19) | -1.3155971e-007 |
| X * Y**4 (SCO XY4 \| C20) | 0 |
| Y**5 (SCO Y5 \| C21) | 4.0503658e-008 |
| X**6 (SCO X6 \| C22) | 1.3439432e-007 |
| X**5 * Y (SCO X5Y \| C23) | 0 |

| | |
|---|---|
| X**4 * Y**2 (SCO X4Y2 \| C24) | 2.5855823e-008 |
| X**3 * Y**3 (SCO X3Y3 \| C25) | 0 |
| X**2 * Y**4 (SCO X2Y4 \| C26) | -2.699141e-008 |
| X * Y**5 (SCO XY5 \| C27) | 0 |
| Y**6 (SCO Y6 \| C28) | 5.31499927e-009 |
| X**7 (SCO X7 \| C29) | 0 |
| X**6 * Y (SCO X6Y \| C30) | -3.738121e-009 |
| X**5 * Y**2 (SCO X5Y2 \| C31) | 0 |
| X**4 * Y**3 (SCO X4Y3 \| C32) | 2.69691705e-012 |
| X**3 * Y**4 (SCO X3Y4 \| C33) | 0 |
| X**2 * Y**5 (SCO S2Y5 \| C34) | 4.84174393e-011 |
| X * Y**6 (SCO XY6 \| C35) | 0 |
| Y**7 (SCO Y7 \| C36) | -1.39752199e-010 |
| X**8 (SCO X8 \| C37) | 4.2757097e-011 |
| X**7 * Y (SCO X7Y \| C38) | 0 |
| X**6 * Y**2 (SCO X6Y2 \| C39) | 1.1630807e-011 |
| X**5 * Y**3 (SCO X5Y3 \| C40) | 0 |
| X**4 * Y**4 (SCO X4Y4 \| C41) | 3.4775484e-011 |
| X**3 * Y**5 (SCO X3Y5 \| C42) | 0 |
| X**2 * Y**6 (SCO X2Y6 \| C43) | 3.6136367e-012 |
| X * Y**7 (SCO XY7 \| C44) | 0 |
| Y**8 (SCO Y8 \| C45) | -5.8509308e-013 |
| X**9 (SCO X9 \| C46) | 0 |
| X**8 * Y (SCO X8Y \| C47) | 0 |
| X**7 * Y**2 (SCO X7Y2 \| C48) | 0 |
| X**6 * Y**3 (SCO X6Y3 \| C49) | 0 |
| X**5 * Y**4 (SCO X5Y4 \| C50) | 0 |
| X**4 * Y**5 (SCO X4Y5 \| C51) | 0 |
| X**3 * Y**6 (SCO X3Y6 \| C52) | 0 |

| | |
|---|---|
| X**2 * Y**7 (SCO X2Y7 \| C53) | 0 |
| X * Y**8 (SCO XY8 \| C54) | 0 |
| Y**9 (SCO Y9 \| C55) | 0 |
| X**10 (SCO X10 \| C56) | 0 |
| X**9 * Y (SCO X9Y \| C57) | 0 |
| X**8 * Y**2 (SCO X8Y2 \| C58) | 0 |
| X**7 * Y**3 (SCO X7Y3 \| C59) | 0 |
| X**6 * Y**4 (SCO X6Y4 \| C60) | 0 |
| X**5 * Y**5 (SCO X5Y5 \| C61) | 0 |
| X**4 * Y**6 (SCO X4Y6 \| C62) | 0 |
| X**3 * Y**7 (SCO X3Y7 \| C63) | 0 |
| X**2 * Y**8 (SCO X2Y8 \| C64) | 0 |
| X * Y**9 (SCO XY9 \| C65) | 0 |
| Y**10 (SCO Y10 \| C66) | 0 |

**Table 9**— Definition of the local surface references in the global coordinate system

| | Origin of surface reference | | | Orientation of the surface |
|---|---|---|---|---|
| | X (mm) | Y (mm) | Z (mm) | Rotation about X-axis θ (°) |
| Surface S19 | 0 | 4.912722 | 5.374900 | 2.588056 |
| Surface S20 | 0 | -5.688113 | 25.091300 | 36.309581 |
| Surface S21 | 0 | -128.220891 | 77.884058 | 18.362678 |
| Surface S22-1 | 0 | -35.523862 | 76.539845 | -13.778904 |
| Surface S23 | 0 | -82.2906 | 81.8565 | 82.6660 |

During the design process, three representative wavelengths, 465nm, 550nm, and 630nm were selected which correspond to the peak emission spectra of the blue, green and red emitters within the selected OLED microdisplay. A total of 21 lenslets in the MLA were sampled with each representing 9 element image points, which added up a total of 189 field samples. To evaluate the image quality, an ideal lens with the same power as the eyepiece is placed at the exit pupil of the system (viewing window), which resulted in a cut-off frequency of 20.83 lp/mm for the final

image, limited by the pixel size of the microdisplay. The optical performance of the designed system was assessed at representative field angles for the three design wavelengths. By changing the power of the tunable lens VFE, the central depth plane could be shifted axially in a large range, for example, from 0 to 3 diopters, without noticeable degeneration of optical performance. Figures 8 through 10 plot the polychromatic modulation transfer function (MTF) for points reconstructed on the CDP set at the depth of 3, 1, and 0 diopters, respectively. For each CDP position, two sets of MTFs were plotted, one for fields corresponding to the on-axis MLA and one for fields correspond to the furthest MLA near the edge.

On the other hand, it is equally important to assess how the image quality of a 3D reconstruction point degrades when the reconstructed image is shifted away from the central depth plane for a specific tunable state. This can be evaluated by shifting the central depth plane a small amount of distance without changing the power of the tunable lens. Figures 11 through 14 plot the polychromatic MTF for reconstructed points shifted away from the CDP by 0.25, 0.5, 0.75, and 1 diopters, respectively. For each depth, two sets of MTFs were plotted, one for fields corresponding to the on-axis MLA and one for fields corresponding to the furthest MLA near the edge.

Figure 15 plots the polychromatic MTF for the 65°x40° FOV. Across the entire the FOV, the see-through path achieved an average MTF value of over 50% at 30 cycles/degree frequency, corresponding to 20/20 normal vision, and nearly 20% at 60 cycles/degree frequency, corresponding to 20/10 vision or 0.5 arc minute of visual acuity.

## CLAIMS

What is claimed is:

1. A head-mounted display integral imaging (InI) system, comprising:
   a microscopic InI unit (micro-InI) configured to create light fields of a selected 3D scene at a selected position along an optical axis of the system;
   a relay group having a vari-focal element (VFE) disposed therein, the relay group disposed on the optical axis at a location so the selected position is an optical conjugate of the relay group, the relay group configured to receive the light fields created by the microscopic InI unit and to create an intermediate 3D scene on the optical axis of the selected 3D scene, the relay group configured to tune the position along the optical axis of the intermediate 3D scene; and
   eyepiece optics for imaging the intermediate 3D scene from the relay group into an exit pupil of the system for viewing by a user of the head-mounted display system.
2. The head-mounted display integral imaging (InI) system of claim 1, wherein the microscopic InI unit (micro-InI) is configured to reproduce full-parallax light fields of a 3D scene having a constrained viewing zone.
3. The head-mounted display integral imaging (InI) system of any one of the preceding claims, comprising a see-through unit in optical communication with the eyepiece optics to transmit a view of a real world to the eyepiece optics for viewing by a user of the head-mounted display system.
4. The head-mounted display integral imaging (InI) system of any one of the preceding claims, wherein the VFE is disposed at a position optically conjugate to the exit pupil.
5. The head-mounted display integral imaging (InI) system of any one of the preceding claims, wherein the relay group comprises along the optical axis: a first lens group and a second lens group with the VFE disposed therebetween.
6. The head-mounted display integral imaging (InI) system of claim 5, wherein the VFE is located at a back focal length of the first lens group.
7. The head-mounted display integral imaging (InI) system of any one of the preceding claims, wherein the field of view of the system is independent of the optical power of the VFE.

8. The head-mounted display integral imaging (InI) system of any one of claims 5–7, wherein the lateral magnification of the relay group is given by $M_R = \frac{1}{(1-z_0\varphi_R)-\frac{\varphi_{vfe}(1-\varphi_2 t_2)+\varphi_2(1+\varphi_1 t_2)}{\varphi_1}}$, where $\varphi_1$, $\varphi_{VFE}$, and $\varphi_2$ are the optical power of the first lens group, VFE, the second lens group, respectively, and where $\varphi_R$ is the compound power of the relay group, $z_0$ is the distance along the optical axis between the front lens group and the selected position, and $t_1$ and $t_2$ are distances along the optical axis between i) the first lens group and the VFE and between ii) the VFE and the second lens group, respectively.
9. The head-mounted display integral imaging (InI) system of any one of the preceding claims, wherein $t_2=1/\varphi_2$ where $t_2$ is the distance along the optical axis between the VFE and the second lens group, and $\varphi_2$ is the optical power of the second lens group.
10. The head-mounted display integral imaging (InI) system of any one of the preceding claims, wherein the relay group is telecentric in object space.
11. The head-mounted display integral imaging (InI) system of any one of the preceding claims, wherein the VFE is disposed on the optical axis at a location such that the compound optical power of the relay group is maintained constant, independent of the optical power of the VFE.
12. The head-mounted display integral imaging (InI) system of any one of the preceding claims, wherein the microscopic InI unit includes a microdisplay and the subtended field angle of the microdisplay through the eyepiece optics is maintained constant, independent of the optical power of the VFE.
13. The head-mounted display integral imaging (InI) system of any one of the preceding claims, wherein the relay group is doubly telecentric.
14. The head-mounted display integral imaging (InI) system of any one of the preceding claims, wherein the eyepiece optics comprises a wedge-shaped freeform prism.
15. The head-mounted display integral imaging (InI) system of any one of the preceding claims, wherein the relay unit is configured to tune the position along the optical axis of the position of a reconstructed 3D virtual scene through the eyepiece by up to 5 diopters.

16. The head-mounted display integral imaging (InI) system of any one of the preceding claims, wherein the focal range of the VFE is 75 – 100 mm.
17. The head-mounted display integral imaging (InI) system of any one of the preceding claims, wherein the focal length of the eyepiece optics is 27.5 mm.
18. The head-mounted display integral imaging (InI) system of any one of the preceding claims, wherein the diagonal field of view of the system is 35°.
19. The head-mounted display integral imaging (InI) system of any one of the preceding claims, wherein the system has an optical resolution as high as 2 arc minutes per pixel.
20. The head-mounted display integral imaging (InI) system of any one of the preceding claims, wherein the microscopic InI unit comprises a micro-lens array of which at least one lens surface is represented by the equation

$$z = \frac{cr^2}{1+\sqrt{1-(1+k)c^2r^2}} + Ar^4 + Br^6 + Cr^8 + Dr^{10} + Er^{12},$$

where z is the sag of the surface measured along the z-axis of a local x, y, z coordinate system, c is the vertex curvature, r is the radial distance, k is the conic constant, A through E are the 4th, 6th, 8th, 10th and 12th order deformation coefficients, respectively.

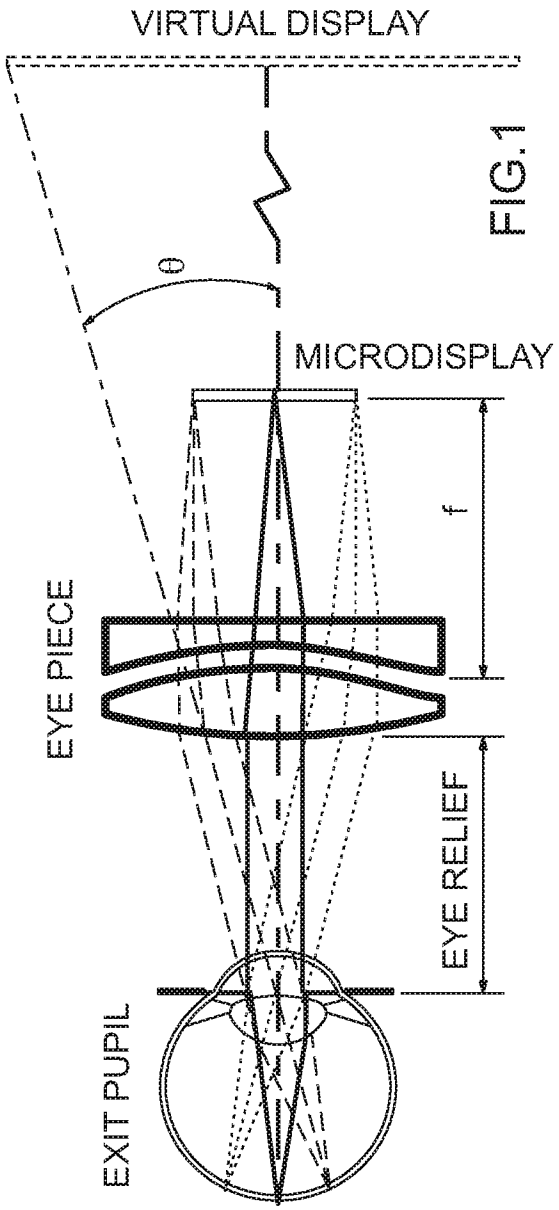
VIRTUAL DISPLAY
θ
MICRODISPLAY
f
EYE PIECE
EYE RELIEF
EXIT PUPIL

FIG.1

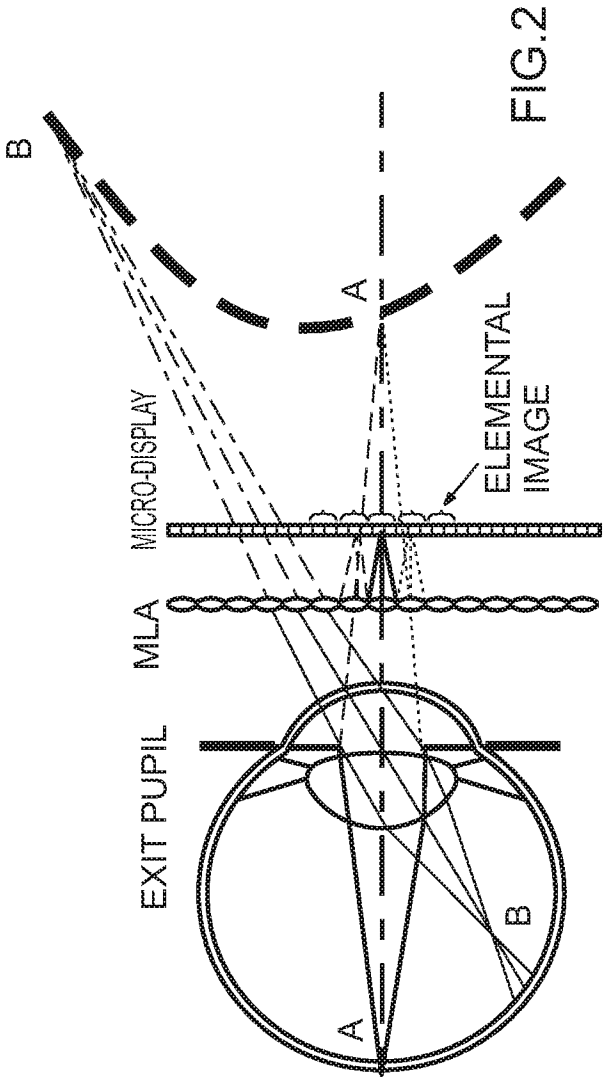
B
A
MICRO-DISPLAY
ELEMENTAL IMAGE
MLA
EXIT PUPIL
B
A

FIG.2

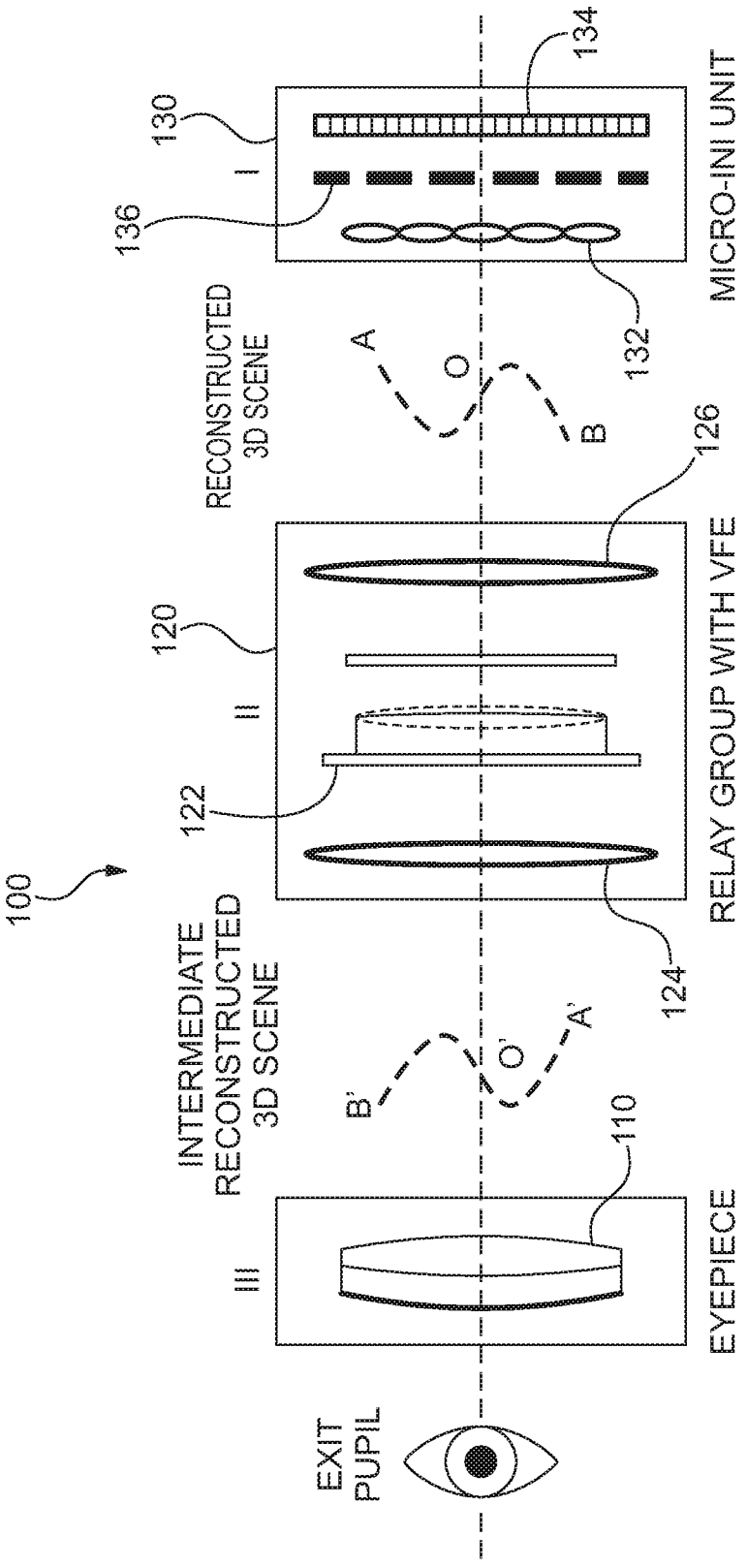
100
EXIT PUPIL
III
EYEPIECE
110
INTERMEDIATE RECONSTRUCTED 3D SCENE
B'
O'
A'
II
120
122
RELAY GROUP WITH VFE
126
124
RECONSTRUCTED 3D SCENE
A
O
B
I
130
136
MICRO-INI UNIT
134
132

FIG.3A

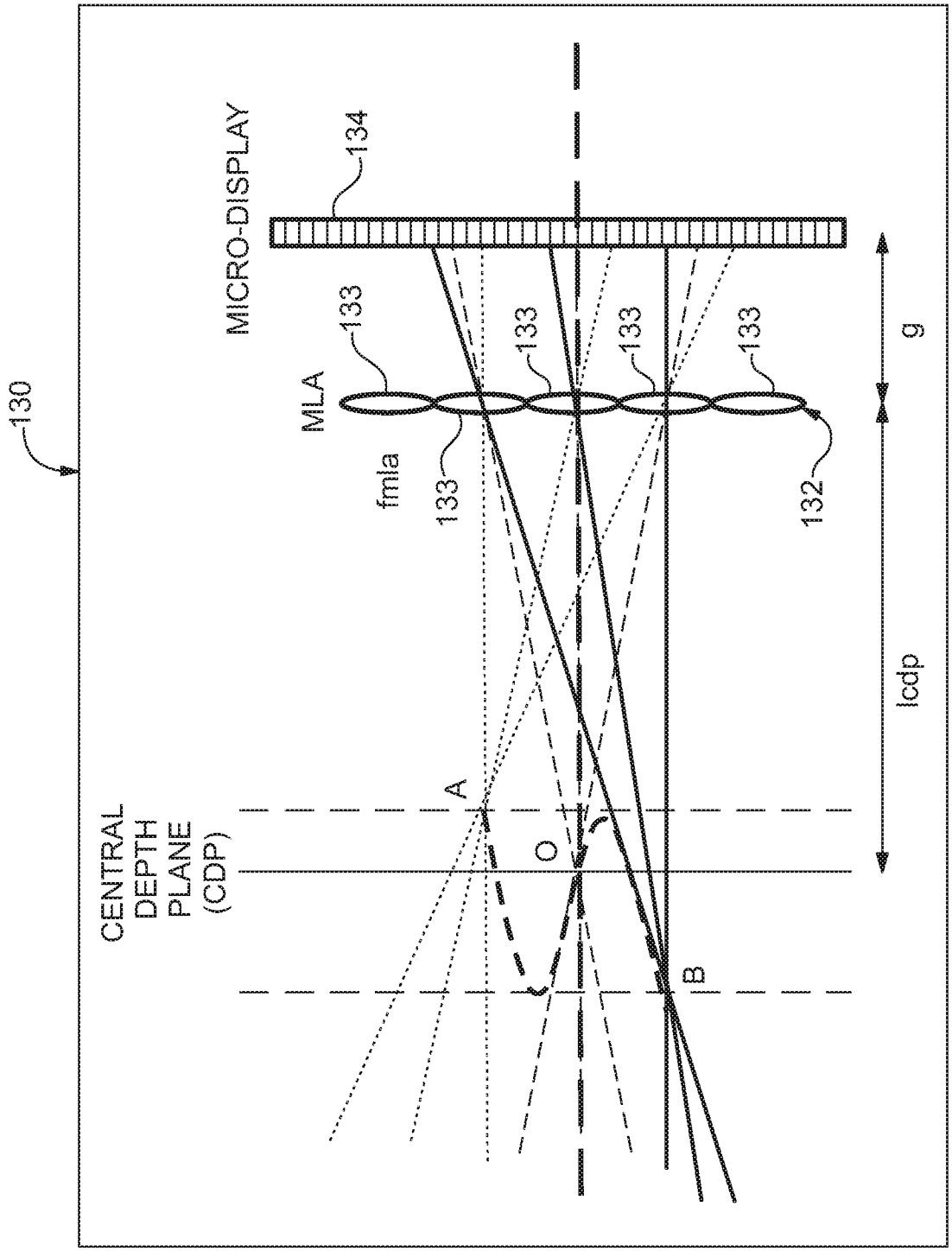
130
MICRO-DISPLAY
134
MLA
133
133
133
133
fmla
133
132
g
lcdp
CENTRAL
DEPTH
PLANE
(CDP)
A
O
B
MICRO-INI UNIT

FIG.3B

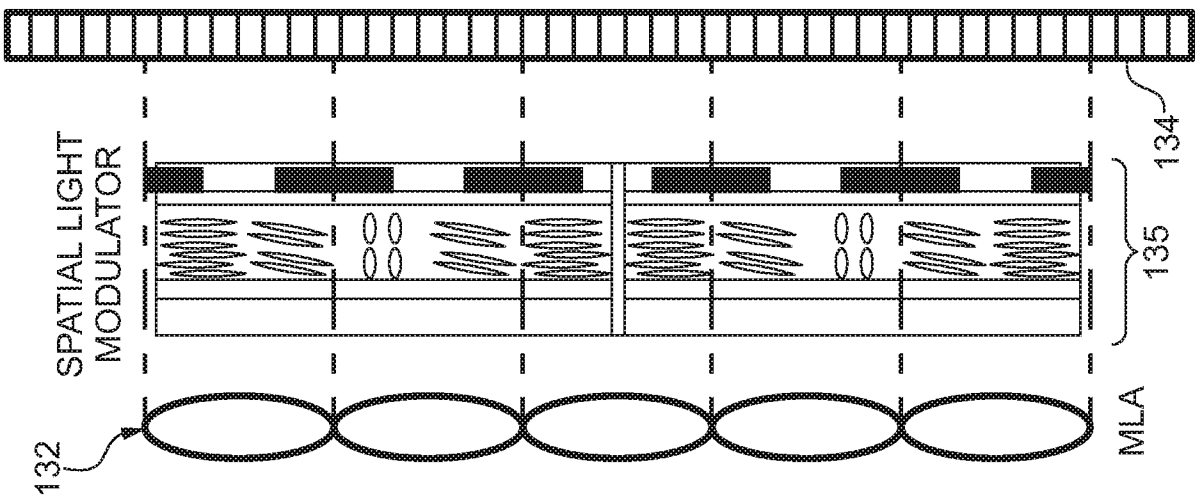
MICRO-DISPLAY
134
SPATIAL LIGHT MODULATOR
135
MLA
132

FIG.4B

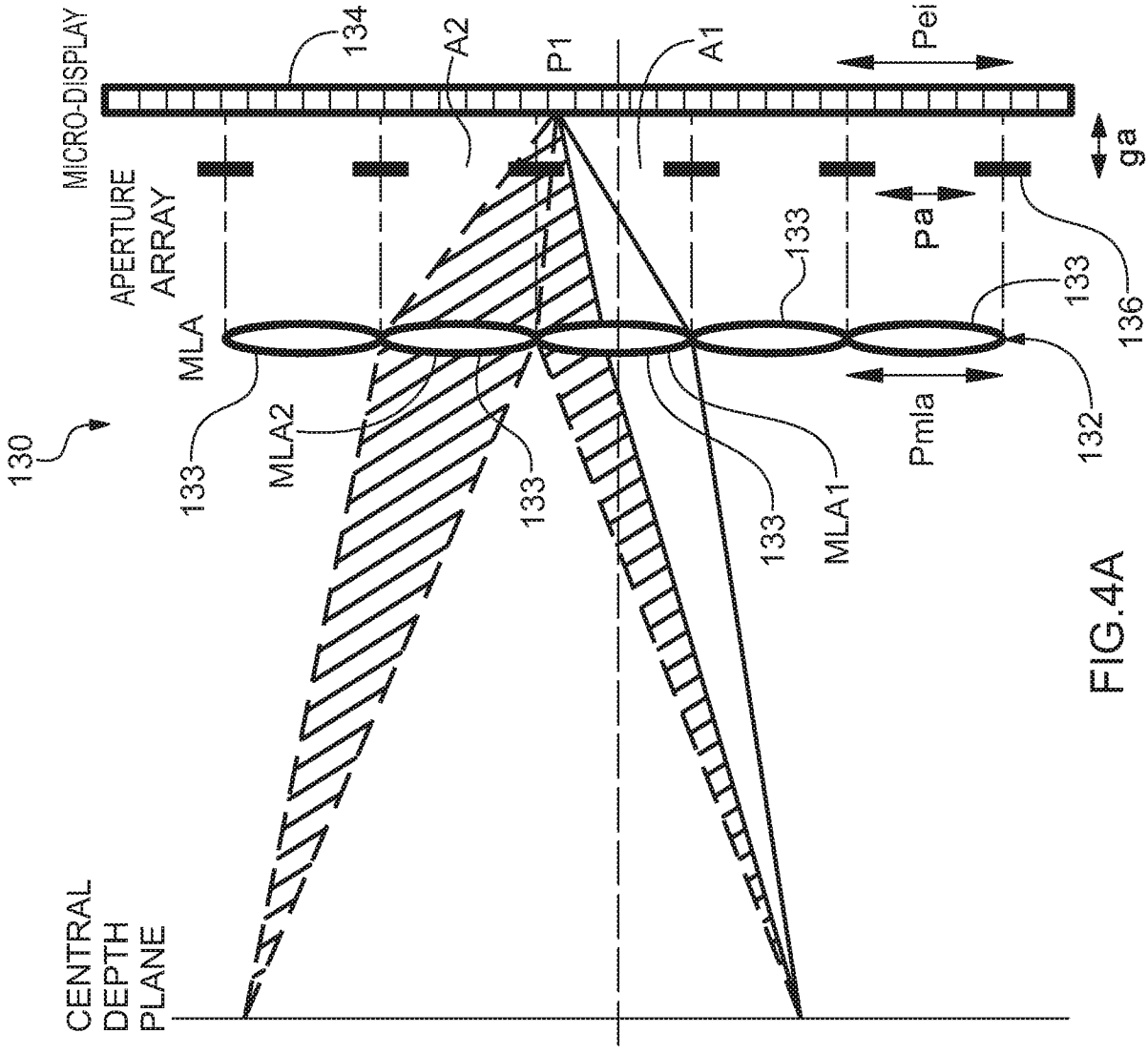
MICRO-DISPLAY
134
A2
P1
A1
Pei
ga
APERTURE ARRAY
MLA
133
Pa
133
136
130
133
MLA2
133
133
MLA1
Pmla
132
CENTRAL DEPTH PLANE

FIG.4A

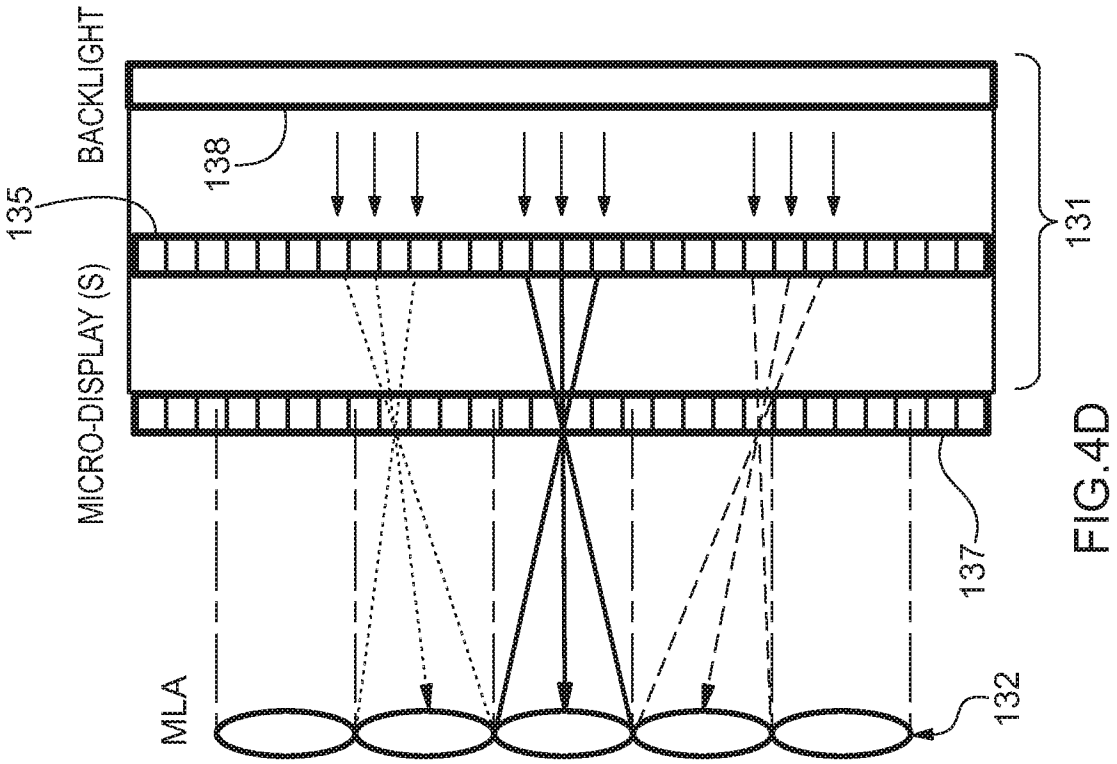
BACKLIGHT
138
135
MICRO-DISPLAY (S)
131
137
MLA
132

FIG.4D

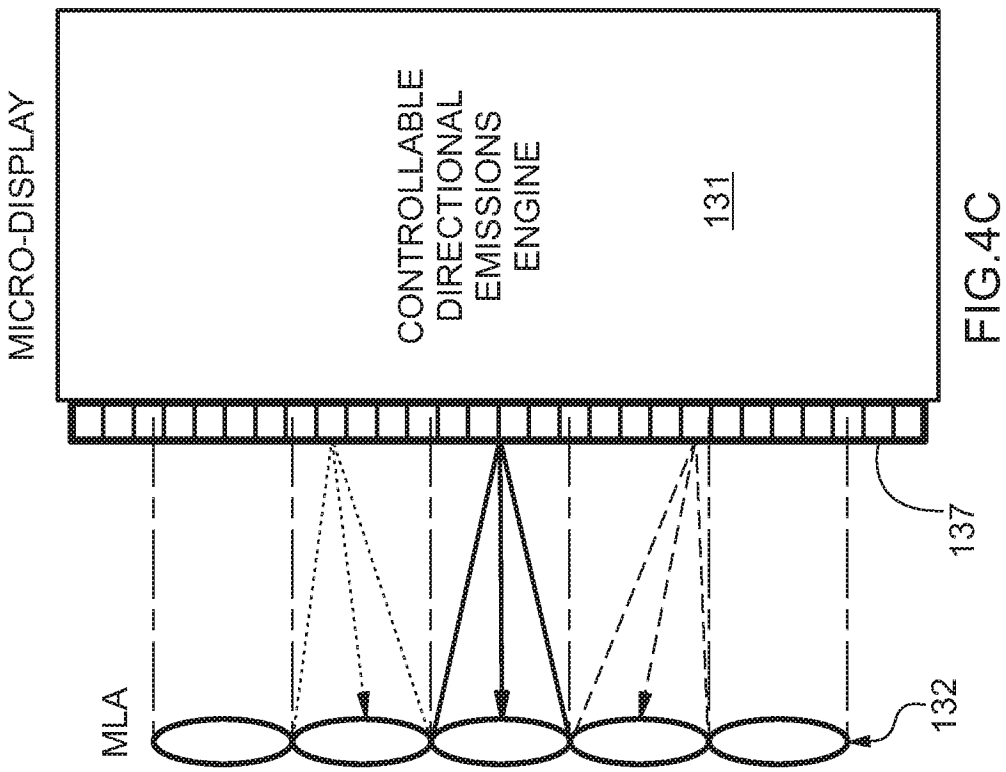
MICRO-DISPLAY
CONTROLLABLE DIRECTIONAL EMISSIONS ENGINE
131
137
MLA
132

FIG.4C

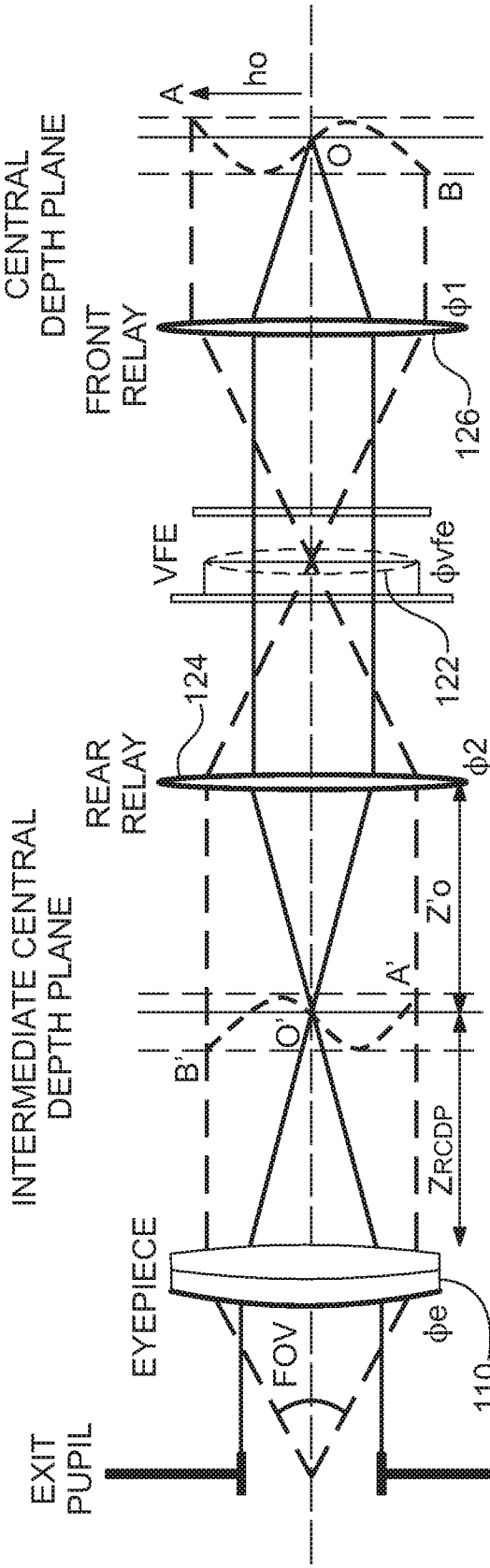
CENTRAL DEPTH PLANE
FRONT RELAY
VFE
REAR RELAY
INTERMEDIATE CENTRAL DEPTH PLANE
EYEPIECE
EXIT PUPIL
A
ho
O
B
Zo
ϕ1
126
t1
ϕvfe
122
120
124
t2
ϕ2
Z'o
A'
O'
B'
t3
ZRCDP
ϕe
110
Zxp
FOV

FIG.5

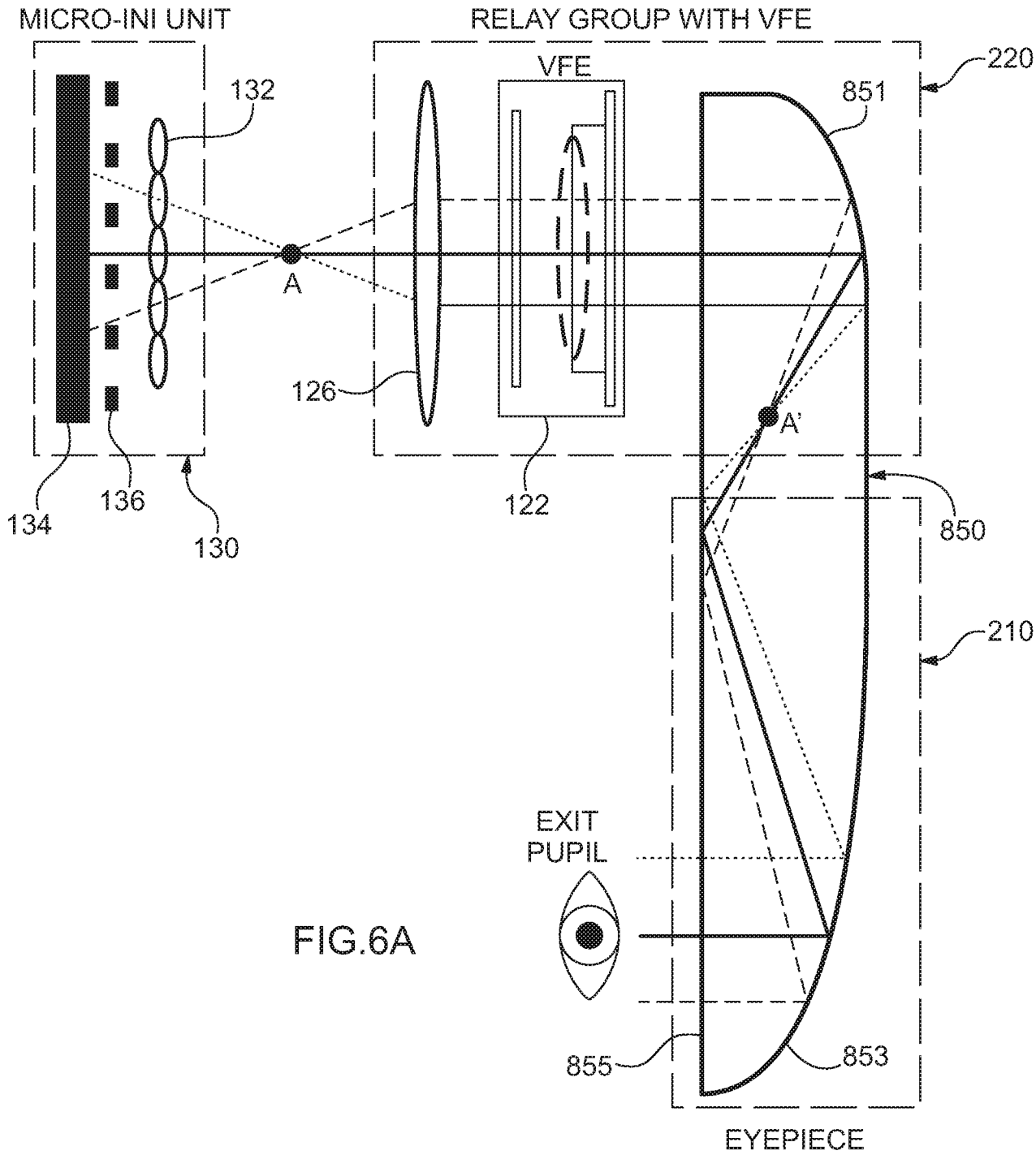
MICRO-INI UNIT
RELAY GROUP WITH VFE
VFE
220
132
851
A
126
A'
122
850
134
136
130
210
EXIT
PUPIL
855
853
EYEPIECE

FIG.6A

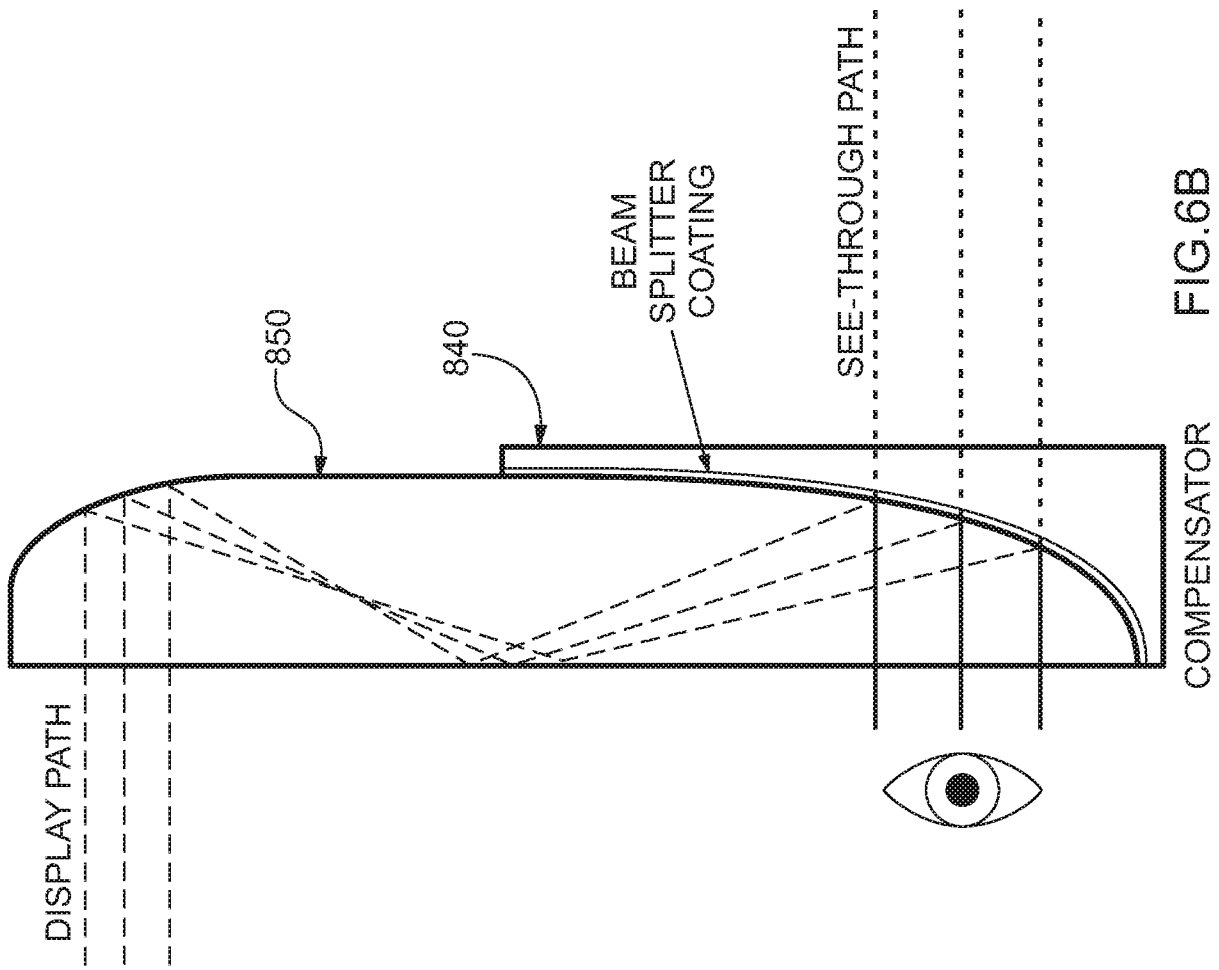
850
840
BEAM SPLITTER COATING
SEE-THROUGH PATH
DISPLAY PATH
COMPENSATOR

FIG.6B

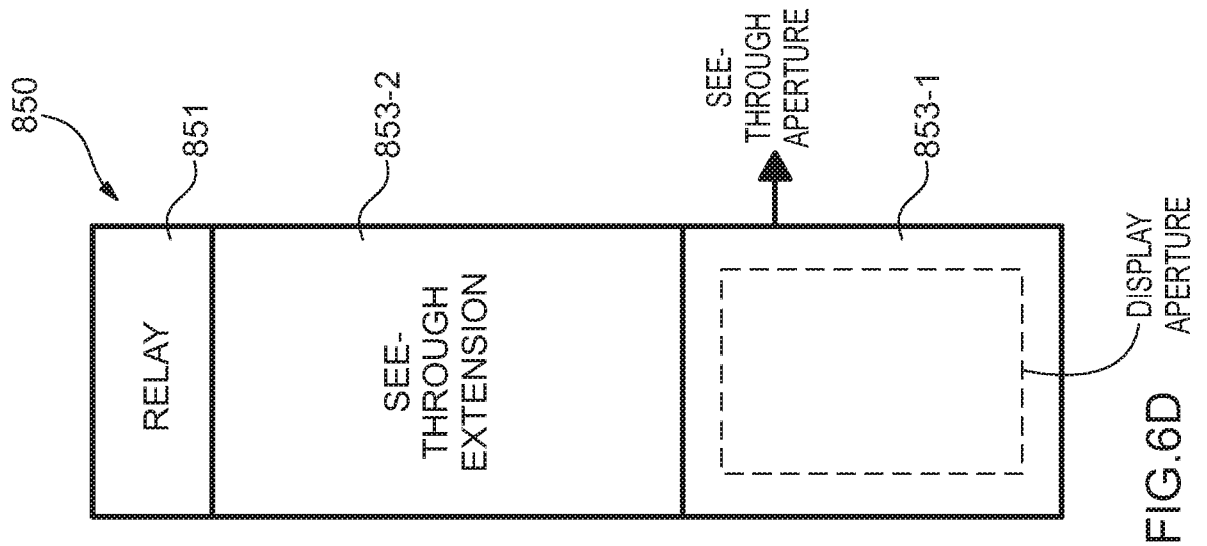
850
851
853-2
SEE-THROUGH APERTURE
853-1
RELAY
SEE-THROUGH EXTENSION
DISPLAY APERTURE

FIG.6D

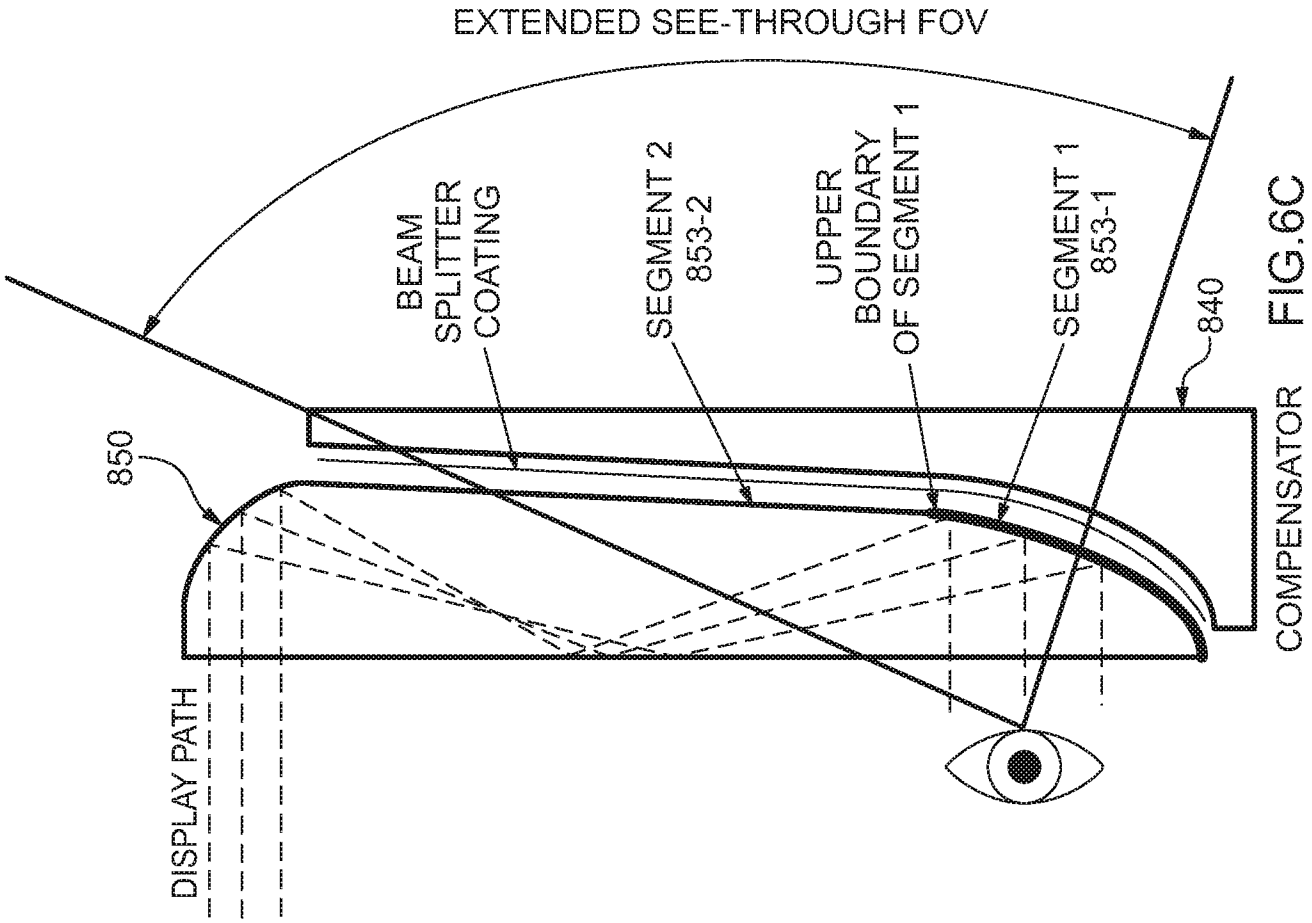
EXTENDED SEE-THROUGH FOV
BEAM SPLITTER COATING
SEGMENT 2 853-2
UPPER BOUNDARY OF SEGMENT 1
SEGMENT 1 853-1
840
850
DISPLAY PATH
COMPENSATOR

FIG.6C

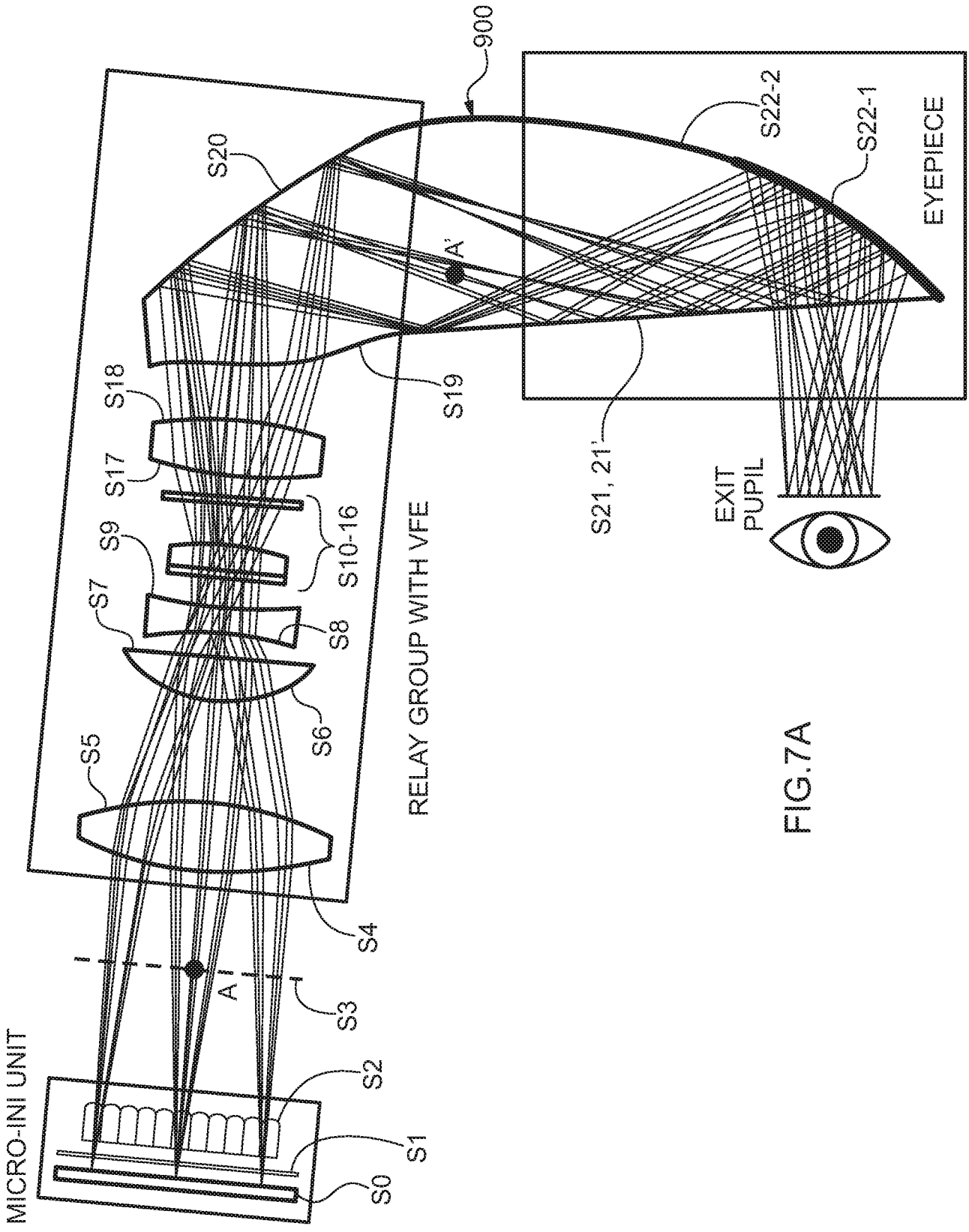
900
S20
S22-2
S22-1
EYEPIECE
A'
S18
S19
S17
S9
S10-16
S7
S8
S6
S5
RELAY GROUP WITH VFE
S21, 21'
EXIT
PUPIL
S4
A
S3
S2
S1
S0
MICRO-INI UNIT

FIG.7A

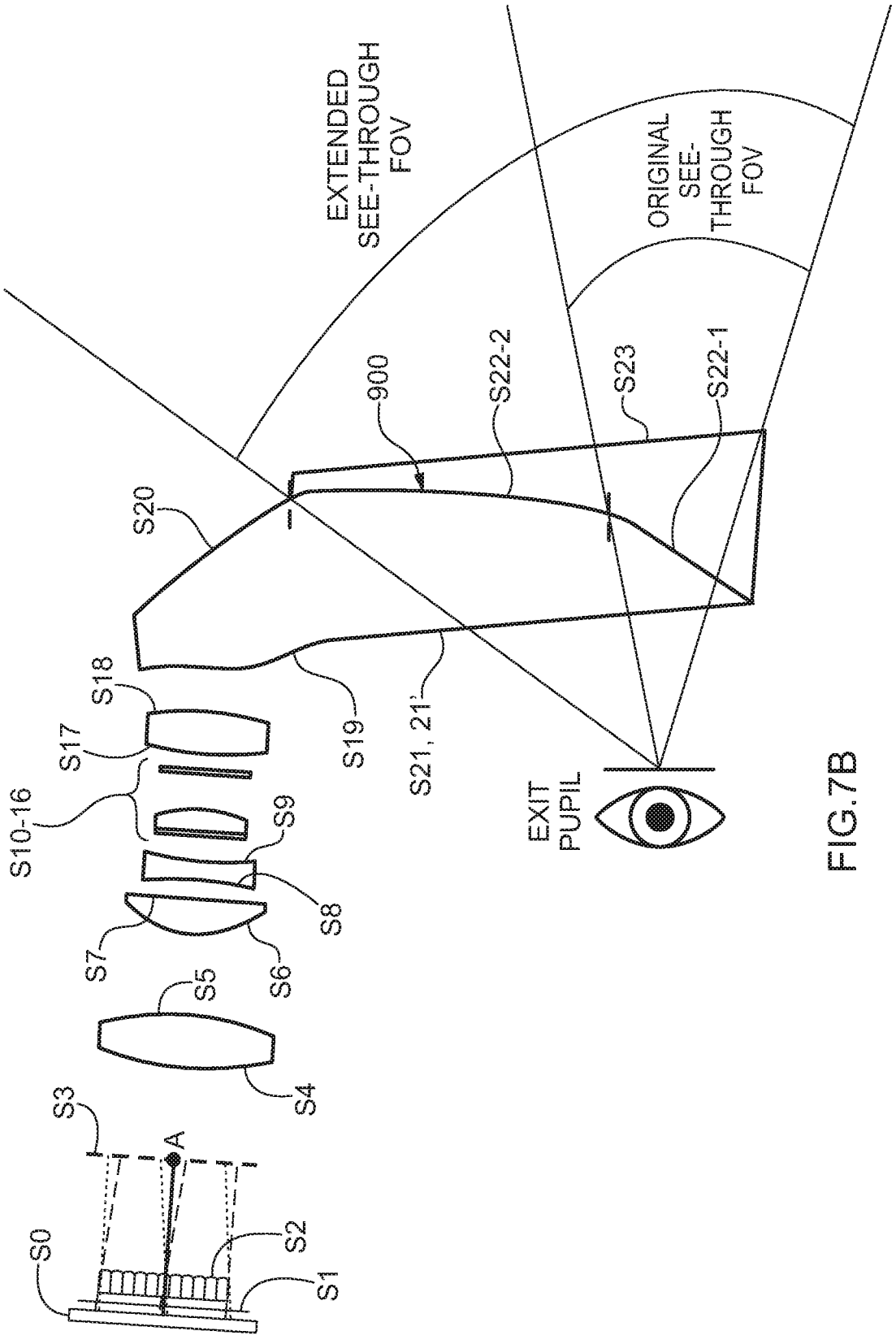
EXTENDED SEE-THROUGH FOV
ORIGINAL SEE-THROUGH FOV
900
S22-2
S23
S22-1
S20
S18
S17
S10-16
S19
S21, 21'
S9
S8
S7
S6
S5
S4
S3
A
S2
S1
S0
EXIT PUPIL

FIG.7B

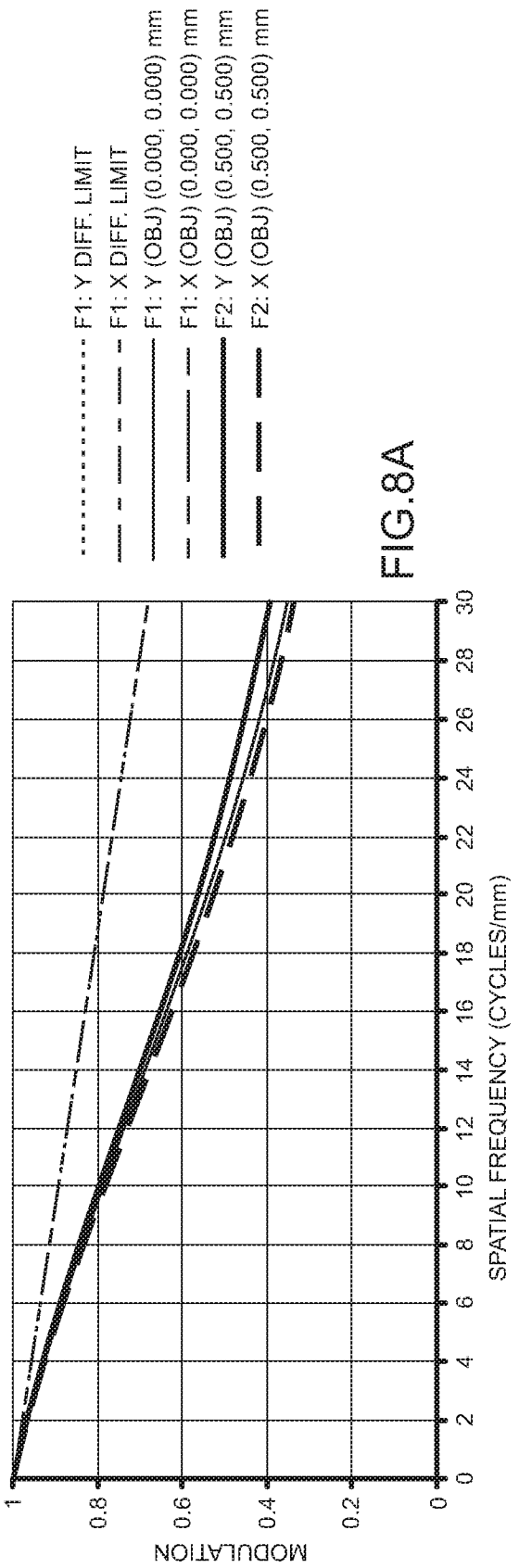
F1: Y DIFF. LIMIT
F1: X DIFF. LIMIT
F1: Y (OBJ) (0.000, 0.000) mm
F1: X (OBJ) (0.000, 0.000) mm
F2: Y (OBJ) (0.500, 0.500) mm
F2: X (OBJ) (0.500, 0.500) mm
MODULATION
SPATIAL FREQUENCY (CYCLES/mm)
0
0.2
0.4
0.6
0.8
1
0
2
4
6
8
10
12
14
16
18
20
22
24
26
28
30

FIG.8A

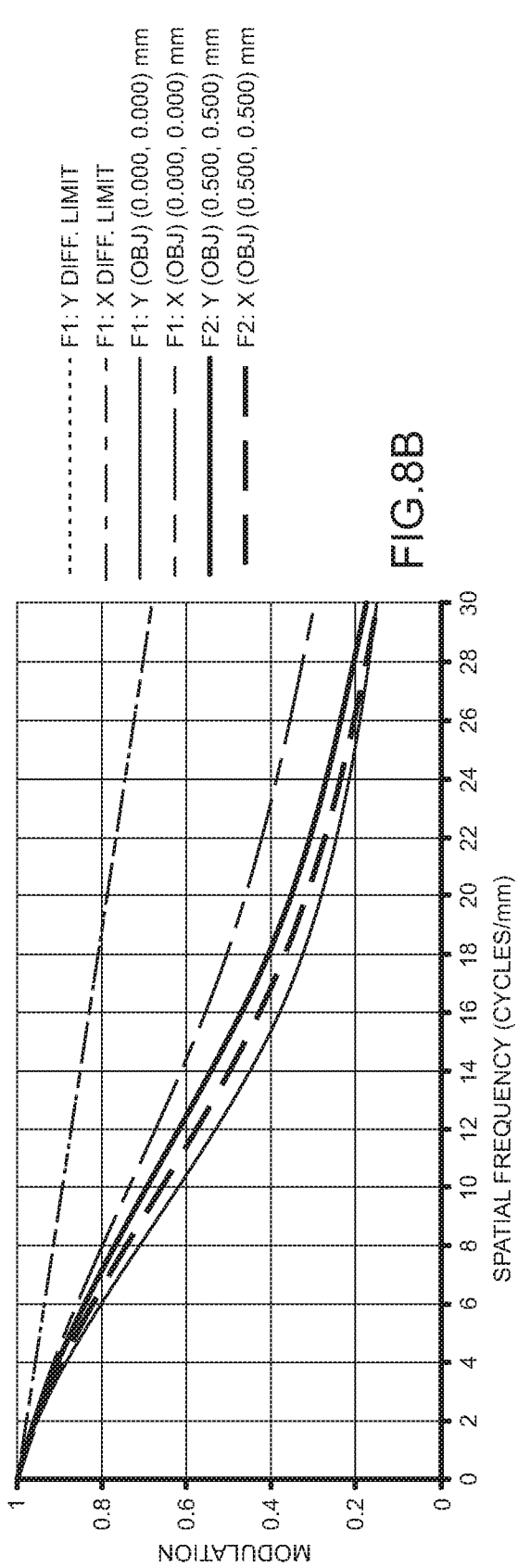
F1: Y DIFF. LIMIT
F1: X DIFF. LIMIT
F1: Y (OBJ) (0.000, 0.000) mm
F1: X (OBJ) (0.000, 0.000) mm
F2: Y (OBJ) (0.500, 0.500) mm
F2: X (OBJ) (0.500, 0.500) mm
MODULATION
SPATIAL FREQUENCY (CYCLES/mm)
0
0.2
0.4
0.6
0.8
1
0
2
4
6
8
10
12
14
16
18
20
22
24
26
28
30

FIG.8B

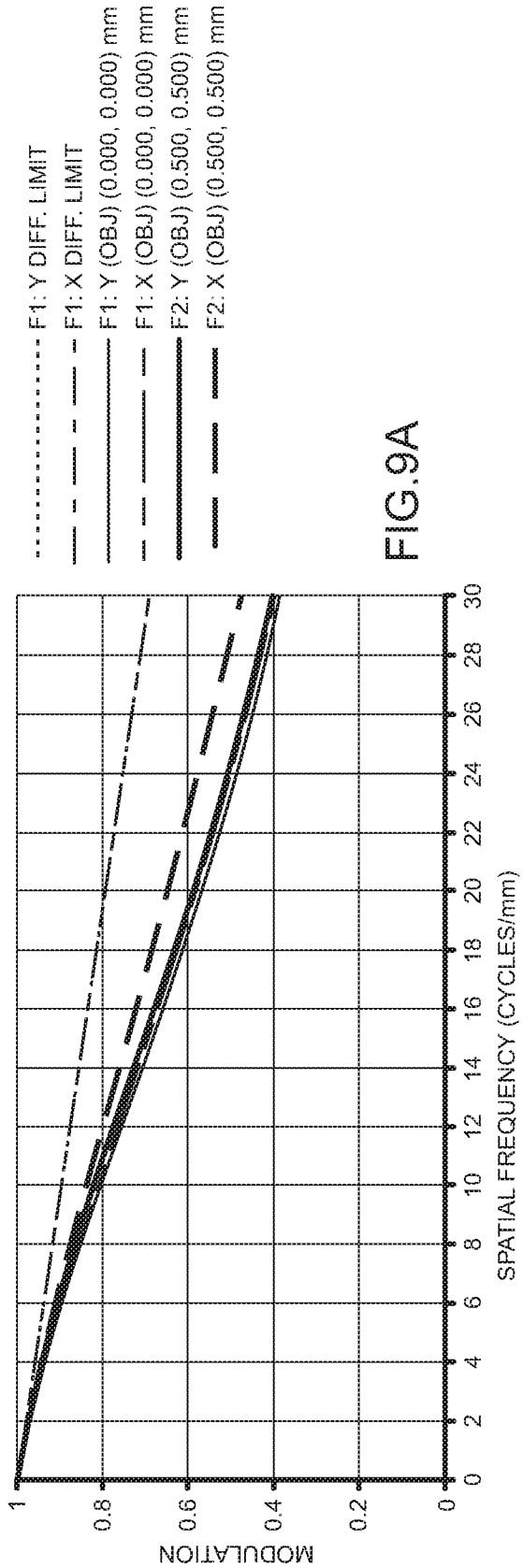
F1: Y DIFF. LIMIT
F1: X DIFF. LIMIT
F1: Y (OBJ) (0.000, 0.000) mm
F1: X (OBJ) (0.000, 0.000) mm
F2: Y (OBJ) (0.500, 0.500) mm
F2: X (OBJ) (0.500, 0.500) mm
MODULATION
SPATIAL FREQUENCY (CYCLES/mm)
0
0.2
0.4
0.6
0.8
1
0 2 4 6 8 10 12 14 16 18 20 22 24 26 28 30

FIG.9A

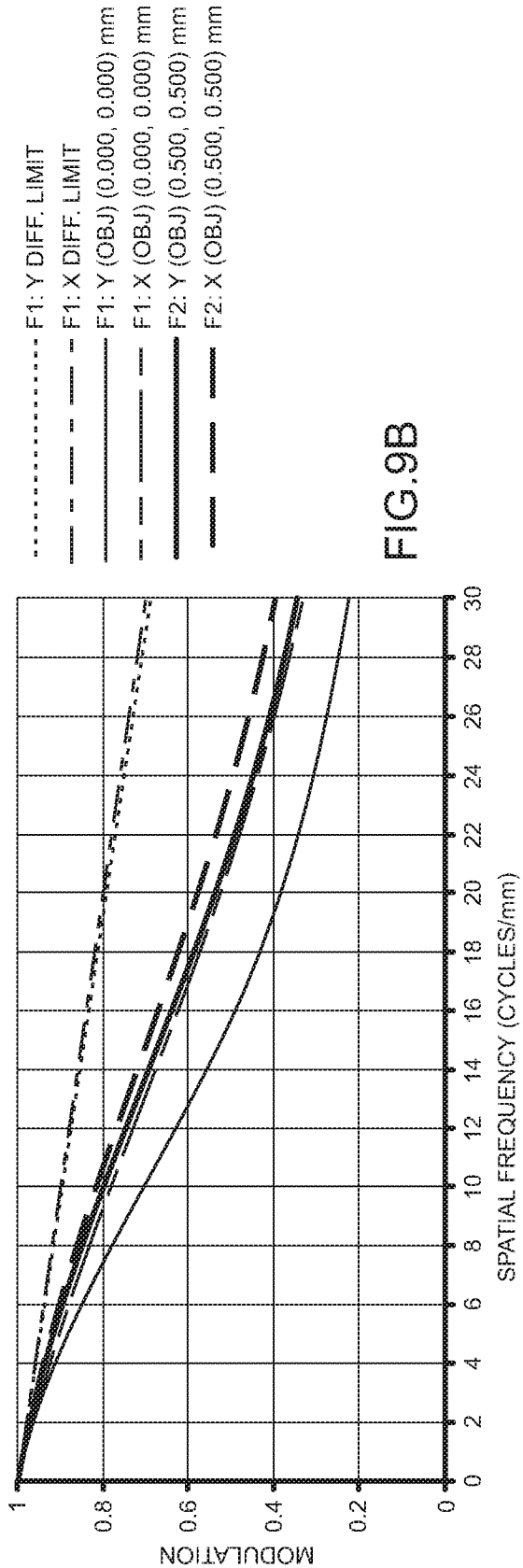
F1: Y DIFF. LIMIT
F1: X DIFF. LIMIT
F1: Y (OBJ) (0.000, 0.000) mm
F1: X (OBJ) (0.000, 0.000) mm
F2: Y (OBJ) (0.500, 0.500) mm
F2: X (OBJ) (0.500, 0.500) mm
MODULATION
SPATIAL FREQUENCY (CYCLES/mm)
0
0.2
0.4
0.6
0.8
1
0 2 4 6 8 10 12 14 16 18 20 22 24 26 28 30

FIG.9B

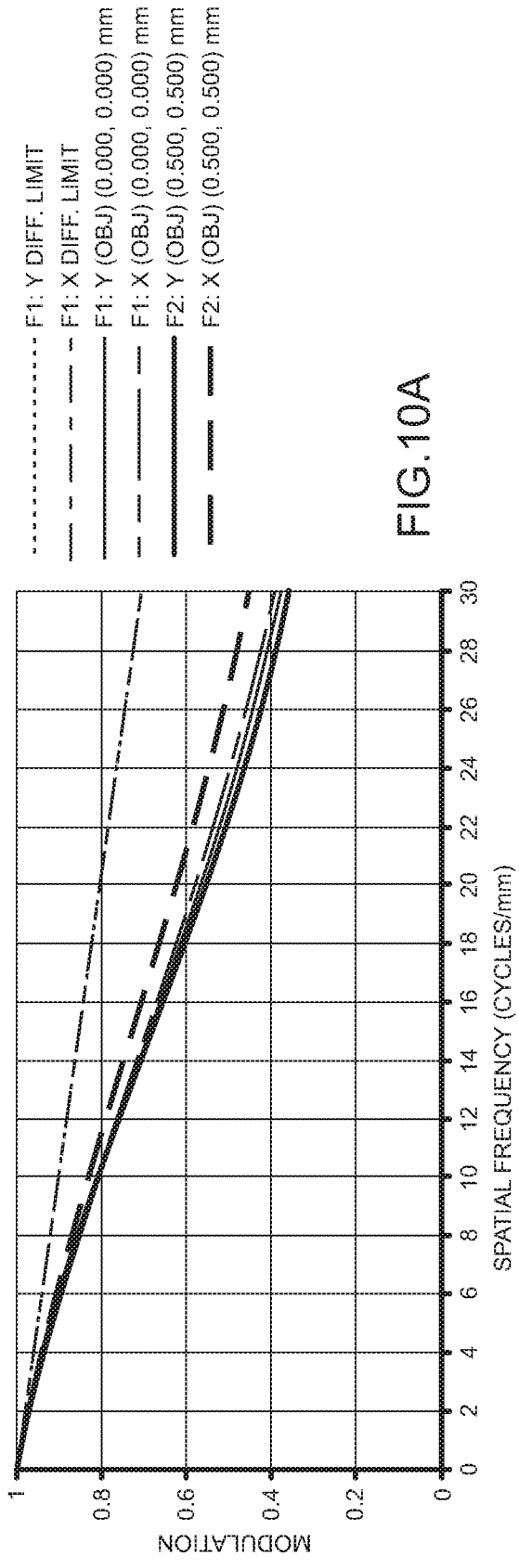


FIG.10A

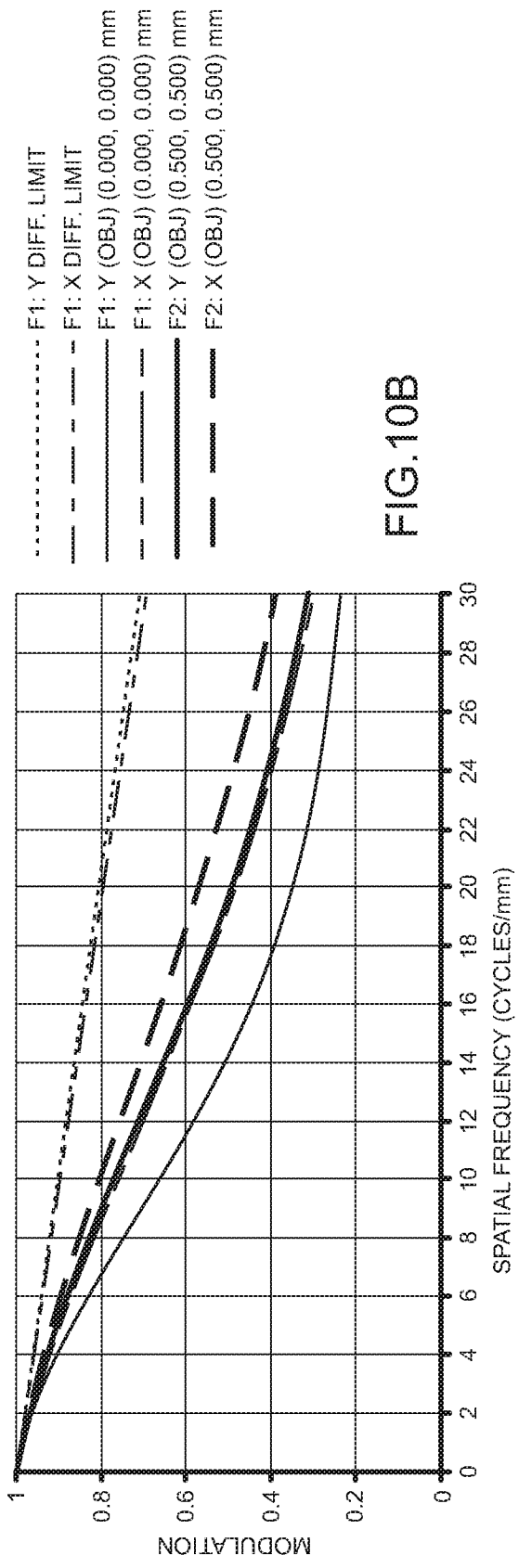


FIG.10B

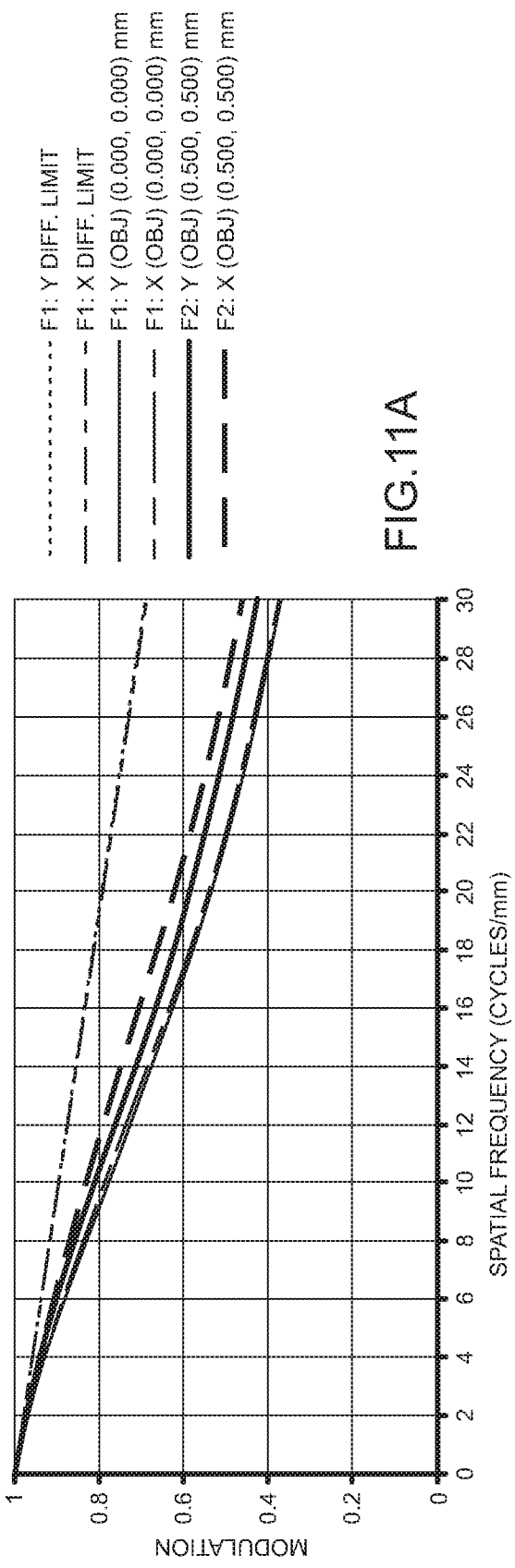


FIG.11A

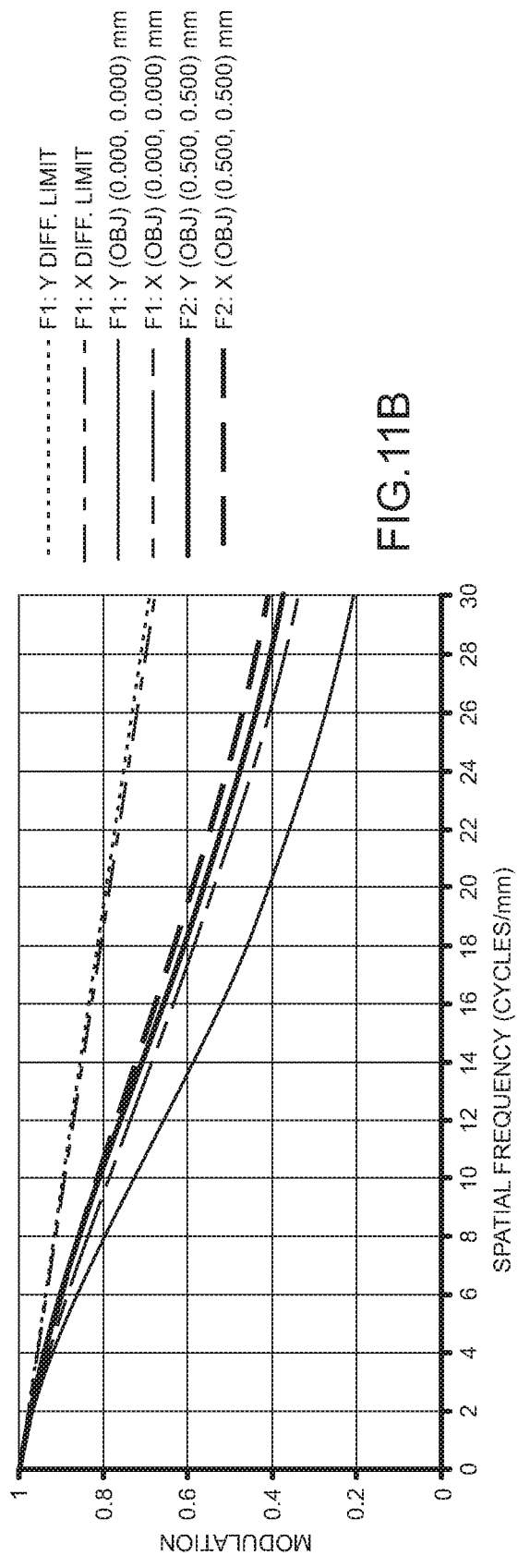


FIG.11B

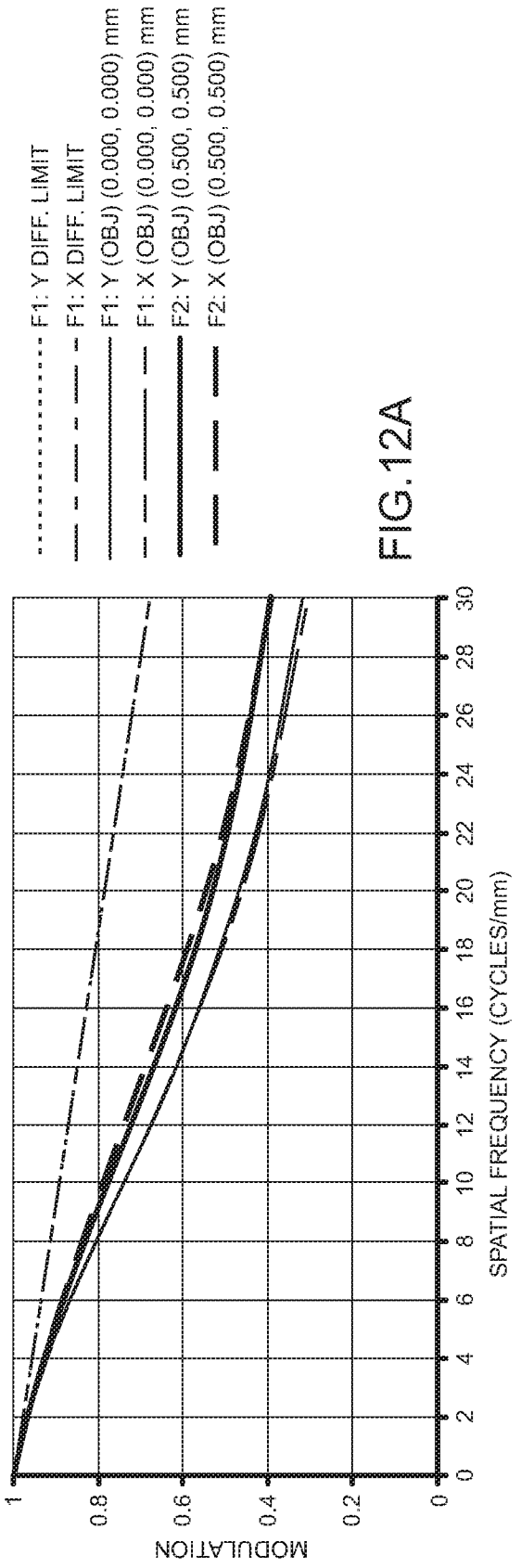


FIG.12A

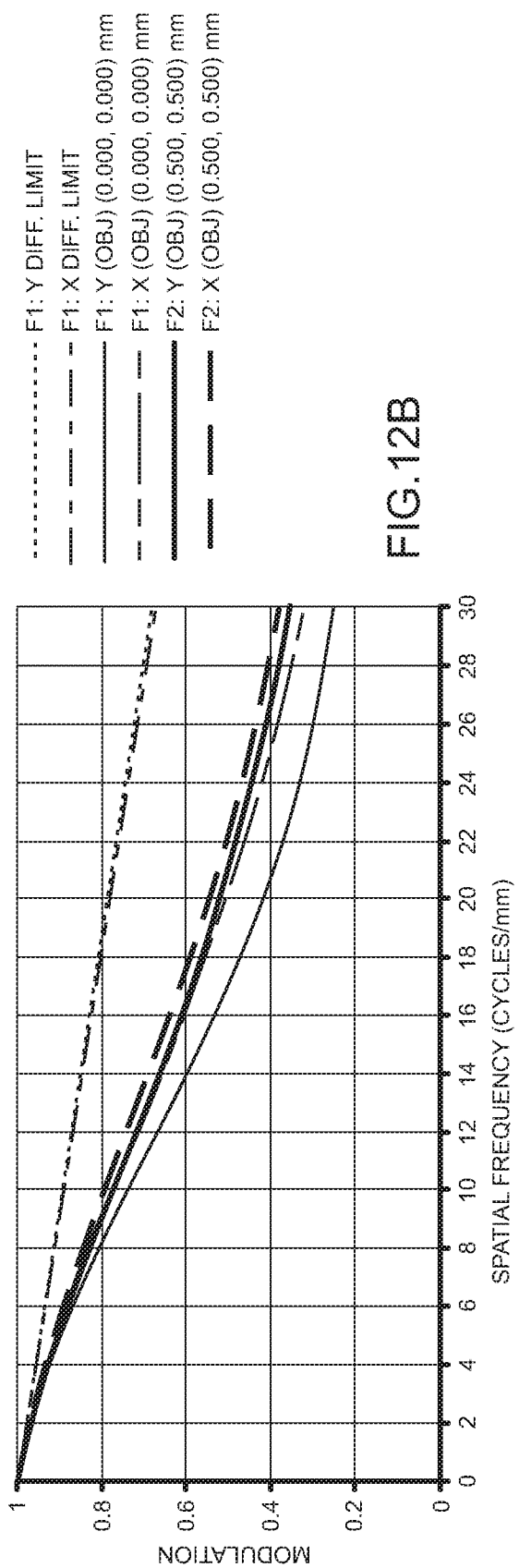


FIG.12B

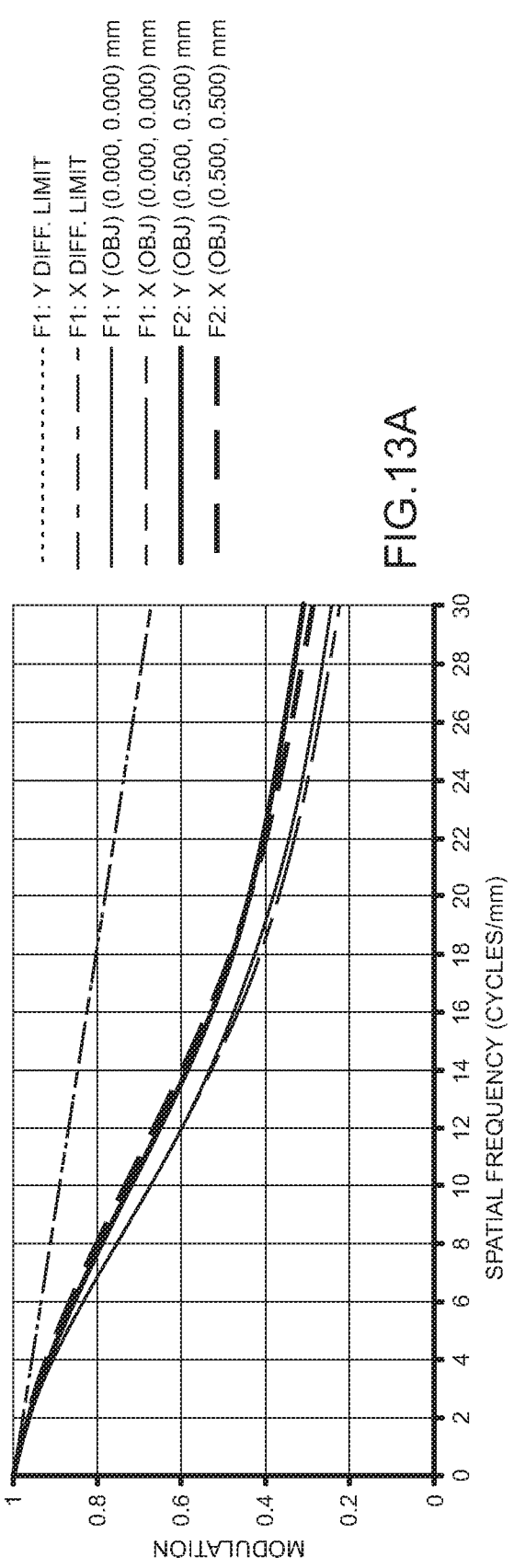


FIG.13A

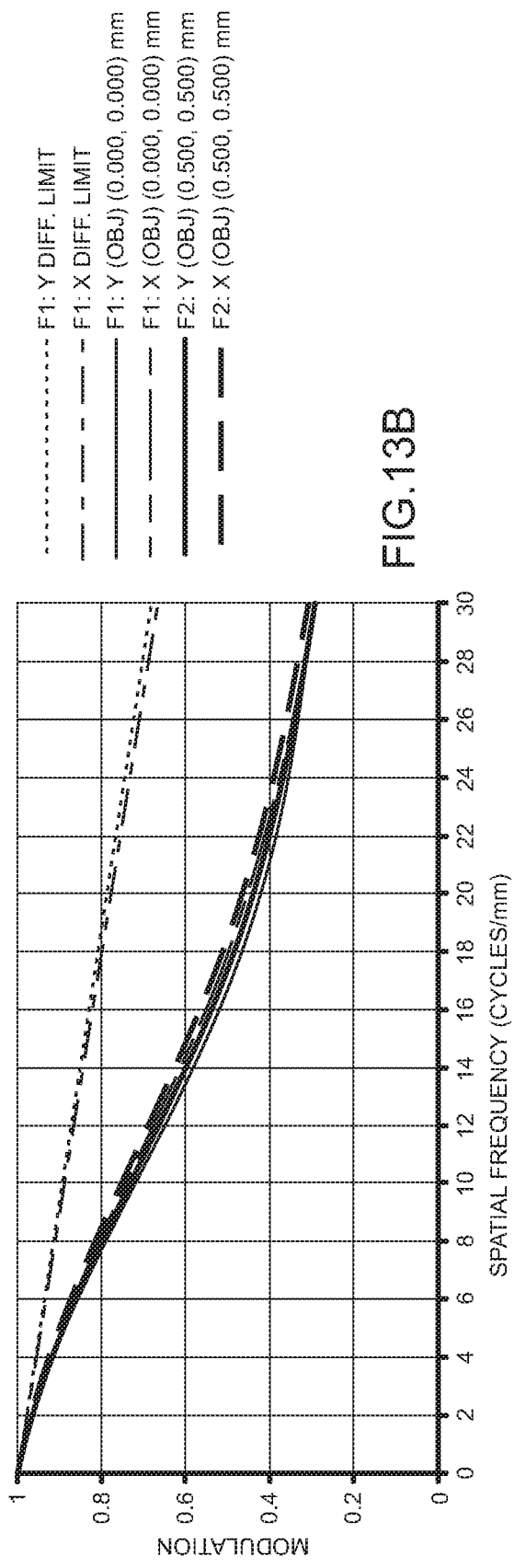


FIG.13B

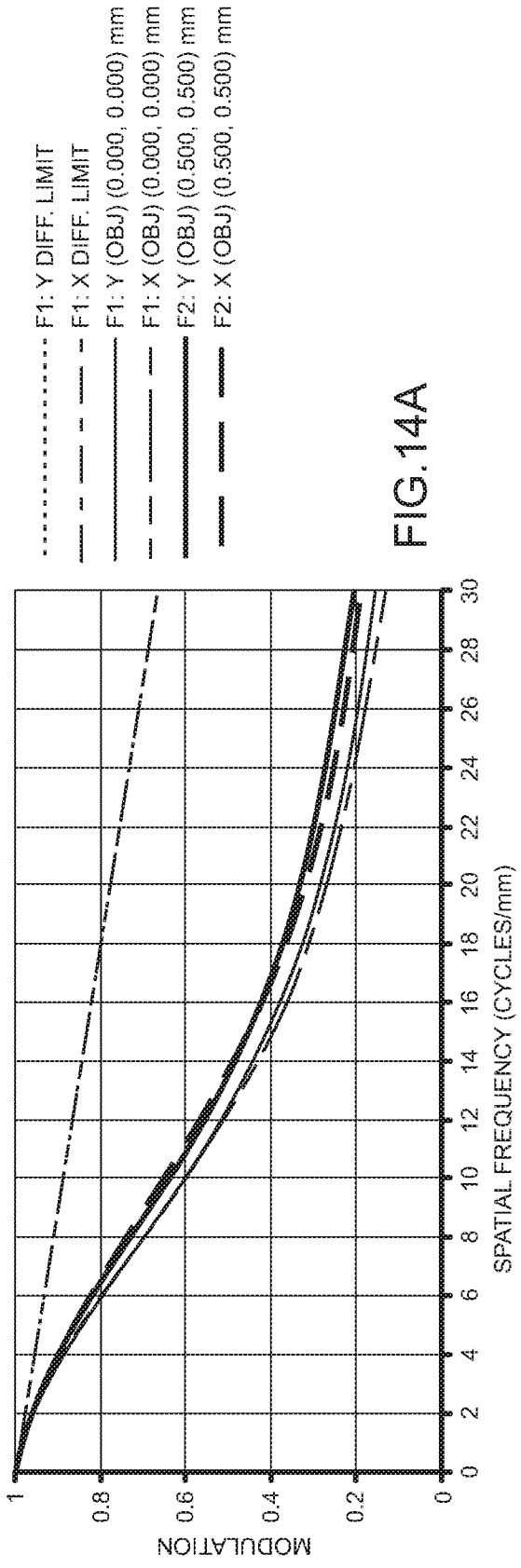


FIG.14A

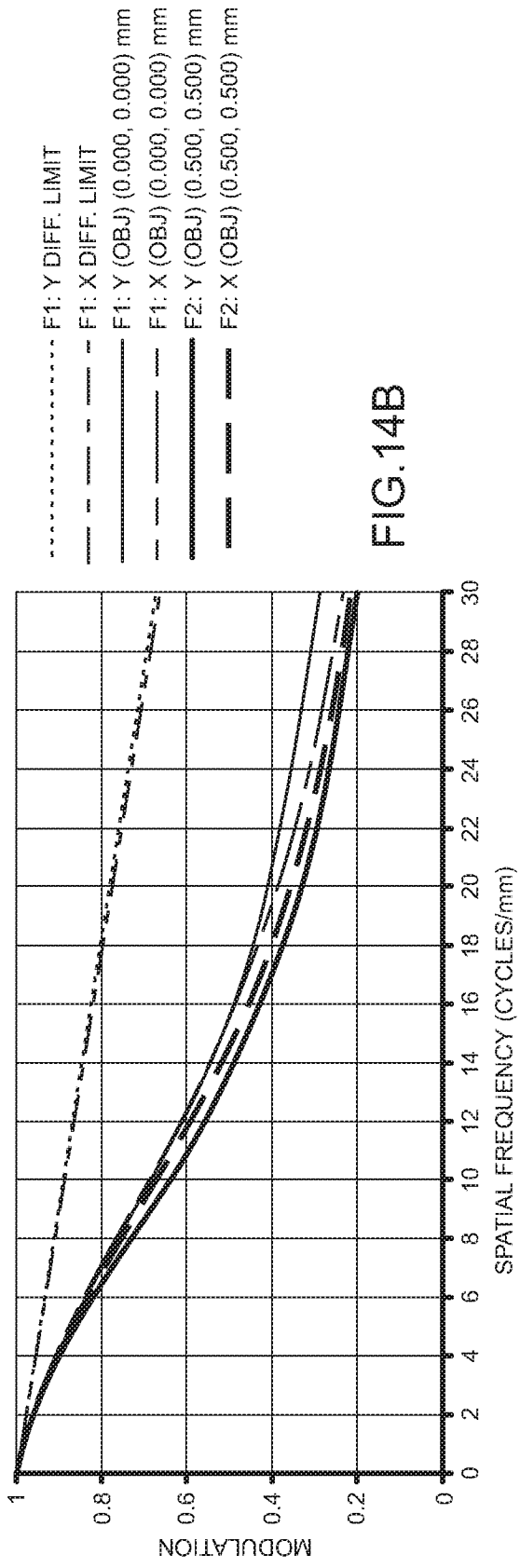


FIG.14B

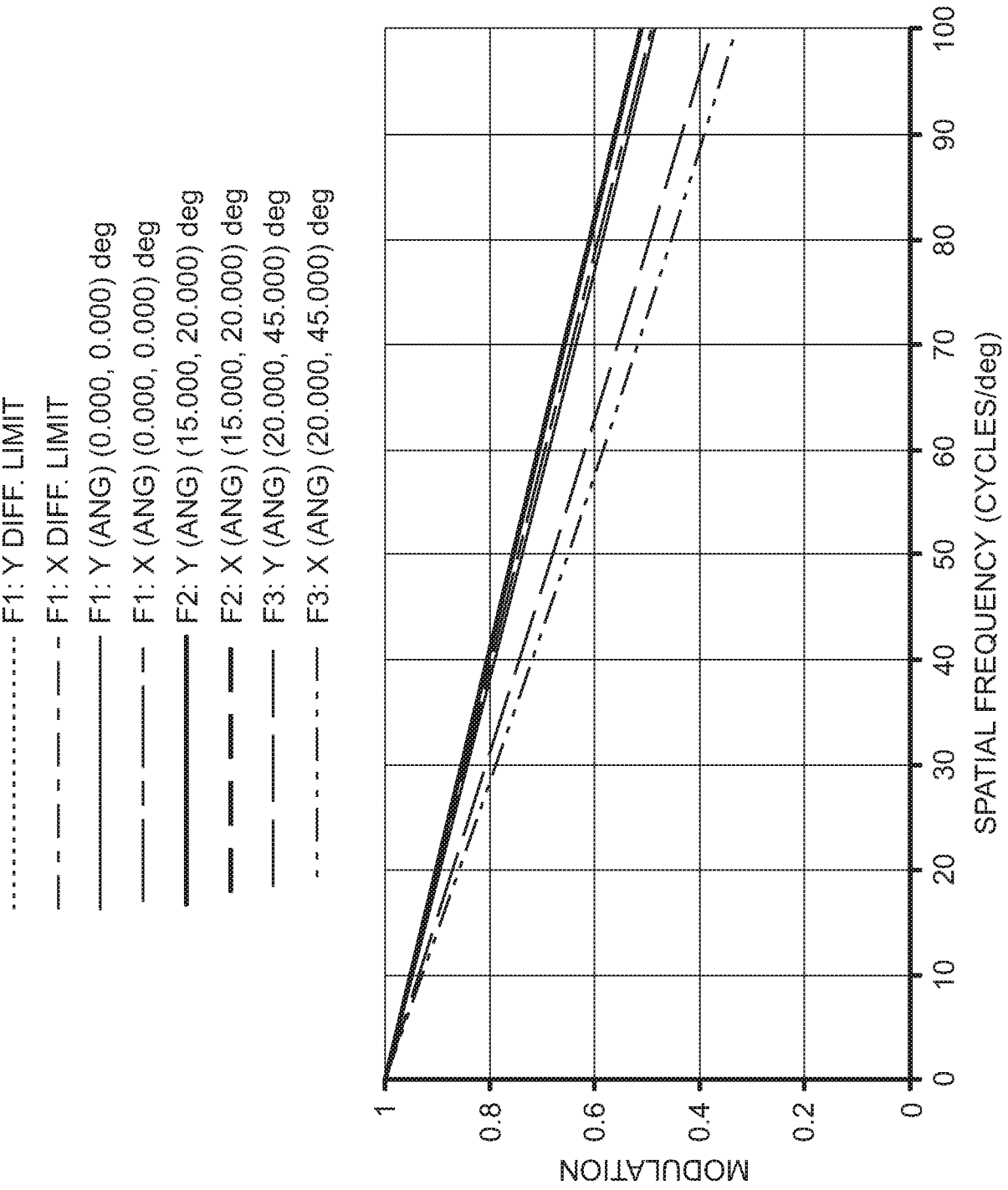
F1: Y DIFF. LIMIT
F1: X DIFF. LIMIT
F1: Y (ANG) (0.000, 0.000) deg
F1: X (ANG) (0.000, 0.000) deg
F2: Y (ANG) (15.000, 20.000) deg
F2: X (ANG) (15.000, 20.000) deg
F3: Y (ANG) (20.000, 45.000) deg
F3: X (ANG) (20.000, 45.000) deg
MODULATION
1
0.8
0.6
0.4
0.2
0
0
10
20
30
40
50
60
70
80
90
100
SPATIAL FREQUENCY (CYCLES/deg)

FIG.15

# INTERNATIONAL SEARCH REPORT

International application No.
PCT/US2018/021087

A. CLASSIFICATION OF SUBJECT MATTER
IPC(8) - G02B 27/01; G02B 17/08; G02B 27/10; G02B 27/22 (2018.01)
CPC - G02B 27/017; G02B 27/01; G02B 15/00; G02B 27/22 (2018.05)

According to International Patent Classification (IPC) or to both national classification and IPC

B. FIELDS SEARCHED

Minimum documentation searched (classification system followed by classification symbols)
See Search History document

Documentation searched other than minimum documentation to the extent that such documents are included in the fields searched
USPC - 345/156; 348/42; 348/44; 359/365; 359/434; 359/479 (keyword delimited)

Electronic data base consulted during the international search (name of data base and, where practicable, search terms used)
See Search History document

C. DOCUMENTS CONSIDERED TO BE RELEVANT

| Category* | Citation of document, with indication, where appropriate, of the relevant passages | Relevant to claim No. |
|---|---|---|
| Y | US 2010/0289970 A1 (WATANABE) 18 November 2010 (18.11.2010) entire document | 1-3 |
| Y | WO 2015/134740 A1 (ARIZONA BOARD OF REGENTS ON BEHALF OF THE UNIVERSITY OF ARIZONA et al) 11 September 2015 (11.09.2015) entire document | 1-3 |
| A | US 3,632,184 A (KING) 04 January 1972 (04.01.1972) entire document | 1-3 |
| A | US 2013/0100524 A1 (MAGARILL et al) 25 April 2013 (25.04.2013) entire document | 1-3 |
| A | US 2015/0277129 A1 (THE ARIZONA BOARD OF REGENTS ON BEHALF OF THE UNIVERSITY OF ARIZONA) 01 October 2015 (01.10.2015) entire document | 1-3 |

☐ Further documents are listed in the continuation of Box C. ☐ See patent family annex.

* Special categories of cited documents:
"A" document defining the general state of the art which is not considered to be of particular relevance
"E" earlier application or patent but published on or after the international filing date
"L" document which may throw doubts on priority claim(s) or which is cited to establish the publication date of another citation or other special reason (as specified)
"O" document referring to an oral disclosure, use, exhibition or other means
"P" document published prior to the international filing date but later than the priority date claimed
"T" later document published after the international filing date or priority date and not in conflict with the application but cited to understand the principle or theory underlying the invention
"X" document of particular relevance; the claimed invention cannot be considered novel or cannot be considered to involve an inventive step when the document is taken alone
"Y" document of particular relevance; the claimed invention cannot be considered to involve an inventive step when the document is combined with one or more other such documents, such combination being obvious to a person skilled in the art
"&" document member of the same patent family

| Date of the actual completion of the international search | Date of mailing of the international search report |
|---|---|
| 04 May 2018 | 21 MAY 2018 |
| Name and mailing address of the ISA/US<br>Mail Stop PCT, Attn: ISA/US, Commissioner for Patents<br>P.O. Box 1450, Alexandria, VA 22313-1450<br>Facsimile No. 571-273-8300 | Authorized officer<br>Blaine R. Copenheaver<br>PCT Helpdesk: 571-272-4300<br>PCT OSP: 571-272-7774 |

# INTERNATIONAL SEARCH REPORT

International application No.
PCT/US2018/021087

**Box No. II Observations where certain claims were found unsearchable (Continuation of item 2 of first sheet)**

This international search report has not been established in respect of certain claims under Article 17(2)(a) for the following reasons:

1. ☐ Claims Nos.:
because they relate to subject matter not required to be searched by this Authority, namely:

2. ☐ Claims Nos.:
because they relate to parts of the international application that do not comply with the prescribed requirements to such an extent that no meaningful international search can be carried out, specifically:

3. ☒ Claims Nos.: 4-20
because they are dependent claims and are not drafted in accordance with the second and third sentences of Rule 6.4(a).

**Box No. III Observations where unity of invention is lacking (Continuation of item 3 of first sheet)**

This International Searching Authority found multiple inventions in this international application, as follows:

1. ☐ As all required additional search fees were timely paid by the applicant, this international search report covers all searchable claims.

2. ☐ As all searchable claims could be searched without effort justifying additional fees, this Authority did not invite payment of additional fees.

3. ☐ As only some of the required additional search fees were timely paid by the applicant, this international search report covers only those claims for which fees were paid, specifically claims Nos.:

4. ☐ No required additional search fees were timely paid by the applicant. Consequently, this international search report is restricted to the invention first mentioned in the claims; it is covered by claims Nos.:

**Remark on Protest**

☐ The additional search fees were accompanied by the applicant's protest and, where applicable, the payment of a protest fee.

☐ The additional search fees were accompanied by the applicant's protest but the applicable protest fee was not paid within the time limit specified in the invitation.

☐ No protest accompanied the payment of additional search fees.